

Palaeoecology of ungulates in northern Iberia during the Late Pleistocene through isotopic analysis of teeth

Mónica Fernández-García^{1,2,3} (*), Sarah Pederzani⁴, Kate Britton⁵, Lucía Agudo-Pérez¹, Andrea Cicero¹, Jeanne Marie Geiling¹, Joan Daura⁶, Montserrat Sanz⁶, Ana B. Marín-Arroyo¹ (*)

1 Grupo de I+D+i EVOADAPTA (Evolución Humana y Adaptaciones durante la Prehistoria), Departamento de Ciencias Históricas, Universidad de Cantabria, 44. 39005 Santander, Spain

2 Departament de Prehistòria, Arqueologia i Història Antiga, Universitat de València, Av. Blasco Ibañez 28, 46010 Valencia, Spain.

3 Institut Català de Paleoecologia Humana i Evolució Social (IPHES-CERCA), zona Educacional 4 Edifici W3, Campus Sescelades URV, 43007 Tarragona, Spain.

4 Spatio-Temporal Isotope Analytics Lab. Department of Geology & Geophysics. University of Utah, Salt Lake City, Utah, USA

5 Department of Archaeology, University of Aberdeen, Aberdeen AB24 3UF, United Kingdom

6 Grup de Recerca del Quaternari (GRQ-SERP), Department of History and Archaeology, Universitat de Barcelona, C/Montalegre 6-8, 08001 Barcelona, Spain.

(*) Corresponding authors: anabelen.marin@unican.es, monica.fegar@gmail.com

Abstract

During the Late Pleistocene, stadial and interstadial fluctuations affected vegetation, fauna, and human groups that were forced to cope with these pronounced spatial-temporal climatic and environmental changes. These changes were especially abrupt during the Marine Isotopic Stage (MIS) 3. Here, we reconstruct the climatic trends in northern Iberia considering the stable isotopic composition of ungulate skeletal tissues found in archaeological deposits dated between 80 to 15 ka cal BP. The carbon and oxygen isotopic composition preserved in the carbonate fraction of tooth enamel provides a reliable and high-resolution proxy of the food and water consumed by these animals, which is indirectly related to the local vegetation, environment, and climate, allowing us to estimate paleotemperatures and rainfall intensity. This study presents new isotope data from 44 bovine, equid, and cervid teeth from five archaeological sites in the Vasco-Cantabrian region (El Castillo, Axlor, Labeko Koba, Aitzbitarte III interior and El Otero,) and one in northeastern Iberia (Canyars), where human evidence is attested from the Mousterian to the Magdalenian. The carbon isotope values reflect animals feeding on diverse C3 plants in open environments, and point to differentiated ecological niches for equids and bovines, especially during the Aurignacian in the Vasco-Cantabrian region. Temperature estimations based on oxygen isotopic compositions and rainfall obtained from carbon isotopic compositions indicate colder and more arid conditions than nowadays for the human occupations from the Late Mousterian to the Aurignacian. The contemporary northeastern Iberia site shows slightly lower temperatures related to an arid period when animals mainly graze in open landscapes. In the Vasco-Cantabrian region, during the MIS2, the Gravettian data reflect a landscape opening, whereas the Magdalenian points to warmer (but still arid) conditions.

Keywords: Middle and Upper Palaeolithic; Neanderthal; Homo sapiens, palaeoecology; geochemistry

1. Introduction

Understanding local and regional climatic variability during the Late Pleistocene in southern Europe is crucial for assessing the potential impact of climate on the adaptation and decline of Neanderthals and the subsequent expansion and resilience of Anatomically Modern Humans during the Upper Paleolithic (e.g., D'Errico and Sánchez Goñi, 2003; Finlayson and Carrión, 2007; Sepulchre et al., 2007; Staubwasser et al.,

45 2018). During the Late Pleistocene, the climatic records demonstrate stadial and interstadial continuous
46 fluctuations during the Marine Isotope Stage 3 (MIS 3, ca. 60-27 ka) and MIS 2 (ca. 27-11 ka). Human
47 groups had to face those episodes, which affected vegetation and fauna to different extents, depending on
48 the region. Northern Iberia is a key study area due to the abundance of well-preserved archaeological caves
49 and rock shelters where, in the last decade, an updated and multidisciplinary approach has been applied to
50 disentangle how changing environmental conditions affected the subsistence dynamics of Middle and
51 Upper Paleolithic hominins. Recent chronological, technological, subsistence studies and ecological
52 reconstructions are revealing a more complex regional panorama than previously known (e.g., Sánchez
53 Goñi, 2020; Vidal-Cordasco et al., 2022; 2023; Timmermann, 2020; Klein et al., 2023).

54 The Vasco-Cantabrian region, located in northwestern Iberia, is subject to the influence of Atlantic climatic
55 conditions, where recently has been evaluated the impact of the glacial-interglacial oscillations during MIS3
56 (Vidal-Cordasco et al., 2022). Modelling of traditional environmental proxies (small vertebrates and pollen)
57 associated to archaeo-paleontological deposits show a progressive shift in the climatic conditions with
58 decreasing temperatures and rainfall levels detected during the late Mousterian (Fernández-García et al.,
59 2023). Ecological alterations have been observed in large mammals, such as niche partitioning between
60 horses and cervids (Jones et al., 2018), a decrease in the available biomass for secondary consumers, and
61 consequently, a reduction in the ungulate carrying capacity ((Jones et al., 2018; Vidal-Cordasco et al.,
62 2022). Cold and arid conditions are observed during the Aurignacian and the Gravettian until the onset of
63 MIS2. Afterwards, during the Last Glacial Maximum (LGM, 23-19 ka), the global climatic deterioration
64 associated with this glacial phase results in colder and more arid conditions in the region, with a
65 predominance of open landscapes. However, this region still provided resources for human survival acting
66 as a refugia with more humid conditions in comparison to the Mediterranean area (Casalheira et al., 2021;
67 Fagoaga, 2014; Fernández-García et al., 2023; Garcia-Ibaibarriaga et al., 2019a; Lécuyer et al., 2021; Posth
68 et al., 2023). By the end of the LGM, a climate amelioration and a moderate expansion of the deciduous
69 forest are documented from the late Solutrean through the Magdalenian (Garcia-Ibaibarriaga et al., 2019a;
70 Jones et al., 2021).

71 In contrast, northeastern Iberia is influenced by the Mediterranean climate. The MIS 3 human settlement in
72 this region have been linked to cooler temperatures and with higher rainfall, compared to the present, but
73 with climatic fluctuations less pronounced compared to the Vasco-Cantabrian region (López-García et al.,
74 2014; Fernández-García et al., 2020; Vidal-Cordasco et al., 2022). Archaeobotanical and small vertebrate
75 evidence indicate relatively stable climatic conditions, but also suggest the persistence of open forests
76 during the Middle to Upper Paleolithic transition, as found in northwestern Iberia (Allué et al., 2018;
77 Ochando et al., 2021). However, certain archaeological records indicate specific climatic episodes, such as
78 increased aridity and landscape opening during Heinrich Stadials 4 and 5 (e.g., Álvarez-Lao et al., 2017;
79 Daura et al., 2013; López-García et al., 2022; Ruffi et al., 2018).

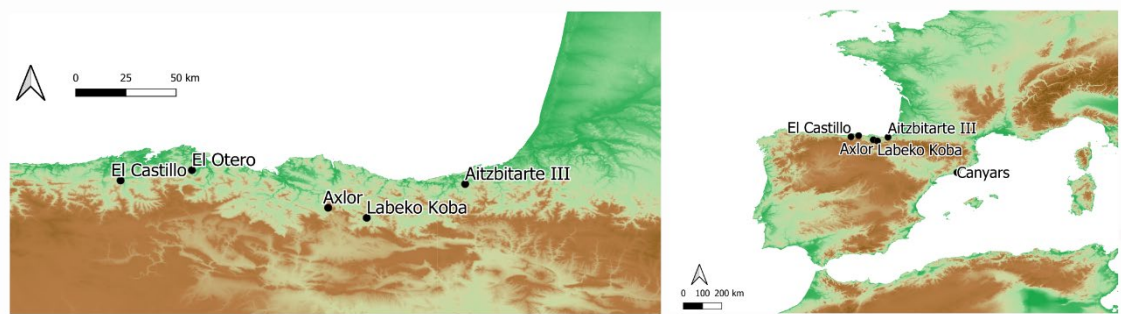
80 These multi-proxy studies have significantly expanded our understanding of the environmental evolution
81 in Iberia, alongside proxies derived from marine core records in Iberia margins (Fourcade et al., 2022;
82 Martrat et al., 2004; Naughton et al., 2007; Roucoux et al., 2001; Sánchez-Goñi et al., 1999, 2009) and
83 other regional paleoclimatic records sourced from local natural deposits (e.g., Pérez-Mejías et al., 2019;
84 Moreno et al., 2010, 2012; González-Sampériz et al., 2020; Ballesteros et al., 2020). However, the
85 availability of proxies enabling the direct connections between these environmental shifts and human
86 activities remains limited.

87 In this study, we investigate the palaeoecological and palaeoenvironmental dynamics in northern Iberia
88 during the late Middle and Upper Paleolithic by measuring the carbon and oxygen isotopic composition of
89 bioapatite carbonates ($\delta^{13}\text{C}_{\text{carb}}/\delta^{18}\text{O}_{\text{carb}}$) preserved in archaeological mammal teeth. These analyses provide
90 high-resolution snapshots of ecological information from animals accumulated during human occupations
91 at the caves. Tooth enamel forms incrementally and does not biologically remodel (Kohn, 2004; Passey
92 and Cerling, 2002), in contrast to other bodily tissues such as bone, which implies that the isotope values
93 measured on them reflect the animal diet and water sources consumed during its mineralisation, around one
94 to two years of life for the species included in our study (bovids, equids, cervids)(e.g., Hoppe et al., 2004;
95 Pederzani and Britton, 2019; Ambrose and Norr, 1993; Luz et al., 1984). The preserved carbon isotope
96 composition relies on animal dietary choices reflecting mainly the type of plant consumed (C3/C4),

97 exposition to light and humidity levels. Otherwise, the oxygen isotope composition reflects mainly the
98 environmental water consumed by animals, directly by drinking or through diet, which reflects isotopic
99 information derived from water sources as well as changes in climatic conditions. Both indirectly provide
100 information on the vegetation and climate that allows estimating past temperatures, rainfall, and moisture
101 on a sub-annual scale, returning isotopic data of the foraging areas where animals were feeding during teeth
102 formation.

103 By analysing the stable isotopic composition of 44 ungulate teeth obtained from 15 archaeological levels
104 directly associated with human occupation, including El Castillo, Axlor, Labeko Koba, Aitzbitarte III
105 interior and El Otero in northwestern Iberia, and Terrasses de la Riera dels Canyars in northeastern Iberia,
106 this study presents novel insights into local and regional environmental and climatic trends associated to
107 human presence during the Late Pleistocene (Fig.1; Fig.2; Appendix A). Specifically, it focuses on the
108 Middle to Upper Paleolithic transition in both areas and the post-LGM period in the Vasco-Cantabrian
109 region.

110 The main objectives of this work are: 1) to assess how regional environmental conditions, including changes
111 in moisture and vegetation cover, but also temperatures and rainfall, are recorded in the stable isotopic
112 composition of tooth enamel; 2) to characterize animal diet and their ecological niches; 3) to obtain
113 quantitative temperature data to compare with available proxies; 4) to characterise seasonal patterns of
114 animals found in the archaeological sites by identifying winter and summer fluctuations.

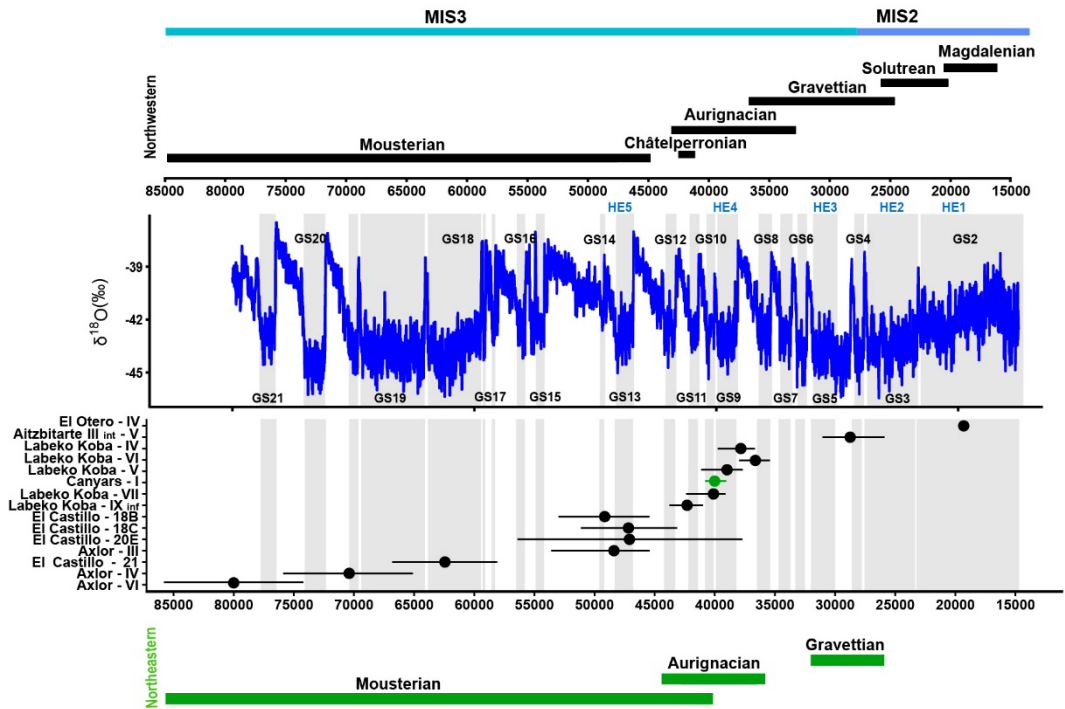


115

116 **Figure 1.** Location of the archaeological sites included in this study. From west to east, in the autonomous
117 community of Cantabria, El Castillo, and El Otero; in the Basque Country, Axlor and Aitzbitarte III interior;
118 in Catalonia, Canyars.

119 2. Archaeological sites and sampled material

120 This study selected a total of 44 ungulate teeth including 25 bovines (*Bos primigenius*, *Bison priscus*,
121 *Bos/Bison* sp.), 14 equids (*Equus* sp. and *Equus ferus*), and five cervids (*Cervus elaphus*) originating from
122 five archaeological sites in the Vasco-Cantabrian region (El Castillo, El Otero, Axlor, Labeko Koba,
123 Aitzbitarte III interior) and one in the northeastern area (Terrasses de la Riera dels Canyars, henceforth
124 Canyars). These teeth were recovered from 15 archaeological levels attributed to the following
125 technocomplexes: Mousterian (n=14), Transitional Aurignacian (n=10), Châtelperronian (n=2),
126 Aurignacian (n=12), Gravettian (n=1) and Magdalenian (n=5) (Table 1 and 2). Archaeozoological studies
127 of the archaeological sites are available (synthesis in Marín-Arroyo and Sanz-Royo, 2022; Daura et al.,
128 2013) and most prove that faunal remains were accumulated by human acquisition during the different
129 cultural phases. The isotopic results of equids teeth and other ungulates bone collagen from El Castillo were
130 previously published by Jones et al. (2019) in combination with the stable isotopes of ungulates from the
131 site, as well as the combined bioapatite carbonate and phosphate analyses of bovines from Axlor (Pederzani
132 et al., 2023). A comprehensive description of each archaeological site is provided in Appendix A.



133
 134 **Figure 2.** Representation of the duration each archaeological level (dots represent the median values, bars
 135 represent 95% confidence intervals for 14C dates and 68% for ESR and OSL dates) related to techno-
 136 complexes in both northwestern (in black) and northeastern Iberia (in green) and the $\delta^{18}O$ record from the
 137 NGRIP (North Greenland Ice Core Project members, 2004; Rasmussen et al., 2014). Grey bands indicate
 138 Greenland Stadials (GS). Dates from EL Castillo (C14 UF, ESR), El Otero (C14 UF), Axlór (C14 UF,
 139 OSL), Labeko Koba (C14 UF), Aitzbitarte III-interior (C14 AMS) and Canyars (C14 UF, ABA, ABOx-
 140 SC) are shown in Appendix B and C.

141

142 **3. Methods**

143 **3.1 Methods: Dating methods**

144 Individual Bayesian age models were built for Canyars, El Castillo, Labeko Koba and Aitzbitarte III interior
 145 based on radiocarbon dates (AMS UF and non-UF, ABOx-SC and ABA pretreatments on bones and
 146 charcoal remains) using OxCal4.4 software (Ramsey, 2009), considering the INTCAL20 calibration curve
 147 (Reimer et al., 2020) (Appendix C). The Bayesian model enables the modification of the calibrated
 148 Probability Distribution Function (PDF) of individual dates based on the existing relative stratigraphic and
 149 other relative age information. A resolution of 20 years was assumed, being a reasonable balance between
 150 required accuracy and computational costs. An order function in the OxCal was used to calculate the
 151 probability that one PDF predated another, providing information to assess synchronicity and temporal
 152 overlap of individual archaeological levels and cultural phases in each of the four separate sites modelled.
 153 Dates were organised into a ‘Sequence,’ and chronological information for each level was grouped into a
 154 single ‘Phase’ with start and end ‘boundaries’ to bracket each archaeological level. The interval between
 155 the start of each level and its end provided the duration of each level. In all cases, convergence was greater
 156 than 95%. CQL codes, individual Bayesian models and modelled dates per site are reported in Appendix
 157 C.

158 No chronological models were built for El Otero because only a single date was obtained for level IV and
 159 El Castillo levels 20E and 21 (ESR dated) and Axlór levels III, IV and VI (OSL dated) because dates go

160 beyond the limit of the radiocarbon. To show the duration of these levels in combination with the other
 161 sites and levels, each of these dates was estimated by adding and subtracting the sigma (68% Confidence
 162 Interval) from the uncalibrated date. In this way, we estimated the duration of these levels to be beyond 55
 163 ka cal BP.

164 3.2 Tooth sampling

165 All teeth included were sequentially sampled to reconstruct the complete $\delta^{18}\text{O}_{\text{carb}}$ and $\delta^{13}\text{C}_{\text{carb}}$ intratooth
 166 profiles based on enamel carbonate bioapatite. Intratooth sequential sampling was applied to the second
 167 and third molars and third and fourth premolars. Bovine and horse teeth sampled exceeded 3-4 cm of crown
 168 height to ensure that at least a one-year isotopic record of animal life was obtained (Britton et al., 2019;
 169 Hoppe et al., 2004). Samples were taken perpendicular to the growth axis on the tooth where the enamel
 170 was best preserved, avoiding, whenever possible taphonomic alterations such as cracks or postdepositional
 171 damages. Samples were performed in the buccal face for the lower teeth and the lingual part for the upper
 172 ones. The outermost enamel surface was abraded to remove the superficial enamel, calculus, cementum, or
 173 concretions adhering to the surface to avoid contaminations. The sequential sampling consisted of straight
 174 strips (ca. 8 x 1.5 x 1 mm) covering the width of the selected lobe, approximately every 2-3 mm, from the
 175 crown to the Enamel-Root-Junction (ERJ). The sample depth covered around 75% of the enamel depth,
 176 and dentine inclusion was avoided. A low-revolution variable-speed manual drill was used, equipped with
 177 1 mm diamond-coated drill bits of conical and cylindrical shape. About 10-15mg of enamel powder was
 178 collected in each subsample, generating 693 subsamples for IRMS measurements (see complete intratooth
 179 profiles in Appendix D).

Site	Level - Cultural period	Bovines	Horses	Red deer	Teeth	Subsamples
Axlor	VI - Mousterian	2			2	32
	IV - Mousterian	1			1	12
	III - Mousterian	4			4	62
El Castillo	21A - Mousterian	2	1		3	47
	20E - Mousterian	2	2		4	56
	18C - Trans. Aurignacian	4			4	66
	18B - Trans. Aurignacian	3	2	1	6	93
Labeko Koba	IX inf - Châtelperronian		1	1	2	24
	VII - ProtoAurignacian	3			3	68
	VI - Aurignacian		1		1	16
	V - Aurignacian	1	1		2	39
	IV - Aurignacian		1		1	16
Canyars	I - Aurignacian	2	3		5	76
Aitzbitarte III interior	V - Gravettian	1			1	18
El Otero	IV - Magdalenian		2	3	5	68
TOTAL		25	14	5	44	693

180

181 **Table 1.** Number of teeth sampled by species, archaeological sites and cultural periods.

182

183 3.3 Sample treatment and stable isotope mass spectrometry

184 Several authors have debated the necessity of chemical pre-treatments to remove organic matter and
185 secondary carbonates from bioapatite carbonates before stable isotopic analysis. Some chemical treatments
186 can introduce secondary carbonates, increase carbonate content, and alter the original isotopic signal
187 (Pellegrini and Snoeck, 2016; Snoeck and Pellegrini, 2015). For this reason, in this work, most of the
188 samples were not pretreated except for the equids and cervids samples from Labeko Koba, El Otero and El
189 Castillo that were sampled and pretreated in an earlier phase of the project. The absence of pretreatment
190 can elevate the risk of secondary carbonates (Chesson et al., 2021; France et al., 2020). Nonetheless, any
191 pretreatment method cannot guarantee their complete removal, and the 'side effects' may compromise the
192 final isotopic signal to a greater extent. While variations in pretreatment methods exist among samples in
193 this study, the lack of a universally accepted protocol necessitates careful consideration of any potential
194 isotopic effects resulting from these differences.

195 Pretreatment was followed for above-mentioned samples from fourteen teeth, where around 7 mg of
196 powdered enamel was prepared and pretreated with 3% of sodium hypochlorite (NaOCl) at room
197 temperature for 24 h (0.1 ml/mg sample) and thoroughly rinsed with deionised water, before a reaction with
198 0.1M acetic acid for 4 h (0.1 ml/mg sample) (Balasse et al., 2002; equivalent protocol in Jones et al., 2019).
199 Samples were then thoroughly rinsed, frozen, and freeze-dried. NaOCl is one of the most common agents
200 used for pretreating carbonates and works as a base that removes organic matter by oxidation. Although it
201 is considered one of the most efficient agents for removing organic matter, it can induce the absorption of
202 exogenous carbonates, such as atmospheric CO₂ and secondary carbonates (Pellegrini and Snoeck, 2016;
203 Snoeck and Pellegrini, 2015). It is argued that acetic acid after NaOCl pretreatment can remove exogenous
204 carbonates absorbed during NaOCl application. However, it is unclear if all newly introduced carbonates
205 are finally released and which effect they produce on the original isotopic composition. These samples were
206 analysed in the Godwin Laboratory (Department of Earth Sciences, University of Cambridge). Enamel
207 powder samples were reacted with 100% orthophosphoric acid for 2 h at 70°C in individual vessels in an
208 automated Gasbench interfaced with a Thermo Finnigan MAT253 isotope ratio mass spectrometer. Results
209 were reported in reference to the international standard VPDB and calibrated using the NBS-19 standard
210 (limestone, $\delta^{13}\text{C} = +1.95\text{‰}$ and $\delta^{18}\text{O} = -2.2\text{‰}$; Coplen, 2011) for which the precision is better than 0.08‰
211 for $\delta^{13}\text{C}$ and 0.11‰ for $\delta^{18}\text{O}$.

212 For the non-pre-treated samples, carbon and oxygen stable isotopic ratios were measured using continuous
213 flow-isotope ratio mass spectrometry, specifically a Europa Scientific 20-20 IRMS coupled to a
214 chromatograph, at the Iso-Analytical laboratory in Cheshire, UK. The samples were weighed into clean
215 exetainer tubes after being flushed with 99.995% helium. Phosphoric acid was then added to the samples,
216 and they were allowed to react overnight to ensure the complete conversion of carbonate to CO₂, following
217 the method outlined by Coplen et al. (1983). The reference materials used for VPDB calibration and quality
218 control of the analysis included IA-R022 (calcium carbonate, $\delta^{13}\text{C} = -28.63\text{‰}$, $\delta^{18}\text{O} = -22.69\text{‰}$), NBS-18
219 (carbonatite, $\delta^{13}\text{C} = -5.01\text{‰}$, $\delta^{18}\text{O} = -23.2\text{‰}$), IA-R066 (chalk, $\delta^{13}\text{C} = +2.33\text{‰}$; $\delta^{18}\text{O} = -1.52$). The accepted
220 values of the in-house standards IA-R022 and IA-R066 were obtained by calibrating against IAEA
221 international reference materials, NBS-18 and NBS-19, and NBS-18 and IAEA-CO-1 (Carrara marble, $\delta^{13}\text{C}$
222 = 2.5‰, and $\delta^{18}\text{O} = -2.4\text{‰}$), respectively. Additionally, in-house standards long-term measured were used:
223 ILC1 (calcite, $\delta^{13}\text{C} = 2.13$, $\delta^{18}\text{O} = -3.99\text{‰}$), and Y-02 (calcite, $\delta^{13}\text{C} = 1.48$, $\delta^{18}\text{O} = -9.59\text{‰}$). The analytical
224 precision of quality control standard replicates was better than 0.09‰ for $\delta^{13}\text{C}$ and better than 0.12‰ for
225 $\delta^{18}\text{O}$. The calcium carbonate content test of these samples, ranging between 3.9% and 8.9%, does not
226 indicate a substantial presence of secondary carbonates, considering Chesson et al. (2021). Additionally,
227 phosphate results on samples from Axlor showed $\delta^{18}\text{O}_{\text{carb}} - \delta^{18}\text{O}_{\text{phos}}$ offsets within the expected range for
228 well-preserved samples (Pederzani et al., 2023).

229 3.4 Carbon stable isotopic compositions as environmental and ecological tracers

230 To unravel animal diet and compare the different species, in standardised terms, it is necessary to consider
 231 the enrichment factor (ϵ^*) between $\delta^{13}\text{C}$ obtained by the animal on its diet ($\delta^{13}\text{C}_{\text{diet}}$) and $\delta^{13}\text{C}$ recorded on
 232 enamel carbonates ($\delta^{13}\text{C}_{\text{carb}}$) (Bocherens, 2003; Cerling and Harris, 1999). The ϵ^* estimated for large
 233 ruminant mammals results in an offset of around 14.1‰ between diet and dental enamel, commonly applied
 234 to medium-sized herbivores. However, it is well-known that this offset varies between species, considering
 235 animals' different physiological parameters. Recently, a formal model to predict species-specific diet-
 236 consumer isotopic offsets has been proposed, which uses body mass (BM) and digestive physiology as the
 237 main factors that regulate the ϵ^* (Tejada-Lara et al., 2018). This model proposes the following prediction
 238 equations for ruminant or foregut fermenters (Equation 1: Eq.1) and hindgut fermenters (Eq. 2):

239 (Eq. 1) $\epsilon^* = 2.34 + 0.05 \text{ (BM)}$ $[\text{r}^2=0.78; \text{p-value}=0.008]$

240 (Eq. 2) $\epsilon^* = 2.42 + 0.032 \text{ (BM)}$ $[\text{r}^2=0.74; \text{p-value}=0.003]$

241 This work compares species with different digestive physiology, ruminants for bovines and cervids, and
 242 non-ruminants for equids. The ϵ^* value was adjusted for each animal to avoid bias from digestive
 243 physiology when comparing these species. The following enrichment factors have been used: 14.6‰ for
 244 *Bos taurus* (Passey et al., 2005a), 13.7‰ for *Equus caballus* (Cerling and Harris, 1999), and 13.2‰ for
 245 *Cervus elaphus* (Merceron et al. (2021) following (Eq. 1) for ruminants with a mean body mass of 125 kg.

246 In body tissues, carbon isotopic composition is considered a combination of diet (understood as consumed
 247 food), environment openness (and associated exposure to light), and the amount of precipitation. Assuming
 248 that $\delta^{13}\text{C}$ of past vegetation is close to $\delta^{13}\text{C}_{\text{diet}}$ of ungulates, Lécuyer et al. (2021) proposed to estimate Mean
 249 Annual Precipitations (MAP) from $\delta^{13}\text{C}_{\text{carb}}$, derived from diets based on C3 plants. After transforming
 250 $\delta^{13}\text{C}_{\text{carb}}$ to $\delta^{13}\text{C}_{\text{diet}}$ using the enrichment factors established above, this work suggested transforming this
 251 value to $\delta^{13}\text{C}$ from vegetation ($\delta^{13}\text{C}_{\text{leaf}}$). However, the isotopic composition of animals' diet may not directly
 252 reflect vegetation cover, but rather the food preference of the animal and this approach should be discussed
 253 alongside other environmental data.

254 The MAP estimation is based on least square regression developed by Rey et al. (2013) and based on Kohn
 255 (2010) dataset (Eq.4), which requires first to estimate the $\delta^{13}\text{C}_{\text{leaf}}$ (Eq. 3). The $\delta^{13}\text{C}$ values of atmospheric
 256 CO_2 ($\delta^{13}\text{C}_{\text{atm}}$) are fixed in -7‰ (Lécuyer et al., 2021; Leuenberger et al., 1992; Schmitt et al., 2012).
 257 Atmospheric CO_2 levels have varied throughout the Late Pleistocene, with $\delta^{13}\text{C}_{\text{atm}}$ range between -7 to -
 258 6.4‰ (Eggleston et al., 2016), favouring an age-specific correction approach. However, maintaining
 259 general corrections is preferred considering the chronological uncertainty of the studied levels.

260 (Eq.3) $\delta^{13}\text{C}_{\text{leaf}} \text{ (VPDB)} = (\delta^{13}\text{C}_{\text{atm}} - \delta^{13}\text{C}_{\text{diet}}) / [1 + (\delta^{13}\text{C}_{\text{diet}} / 1000)]$

261

262 (Eq.4) $\text{Log1}(\text{MAP}+300) = 0.092(\pm 0.004) \times \delta^{13}\text{C}_{\text{leaf}} + 1.148(\pm 0.074)$

263

264 Additionally, Lécuyer et al. (2021) equation also accounts for the pCO_2 effect on $\delta^{13}\text{C}_{\text{leaf}}$ estimation, which
 265 is expected to result in an offset of +1‰ from current levels (considering that pCO_2 was lower than that
 266 experienced after the deglaciation period). If this correction was not applied, MAP results could be
 267 underestimated by -150mm. In agreement with Lécuyer et al. (2021) appreciation, these MAP estimations
 268 are a preliminary approximation and should be cross-validated with other environmental proxies. The
 269 associated uncertainties range from ± 100 to 200 mm, influencing the interpretation of the final values.

270 3.5 Oxygen stable isotope compositions as environmental tracers

271 Stable oxygen isotopes from meteoric water (mainly derived from rainfall) strongly correlate with mean air
 272 temperatures in mid to high latitudes (Dansgaard, 1964; Rozanski et al., 1992) on a regional-to-local scale.
 273 Obligate drinkers, like bovines and horses, acquire this water and record its isotopic composition in their
 274 teeth and bones with a fixed but species-specific offset (Pederzani and Britton, 2019). Considering this two-
 275 step relationship, past climatic conditions can be estimated. However, most of the temperature
 276 reconstructions based on $\delta^{18}\text{O}$ have considered the $\delta^{18}\text{O}$ from the phosphate fraction of bioapatite enamel

277 ($\delta^{18}\text{O}_{\text{phos}}$) to build linear correlations between tooth enamel and drinking water $\delta^{18}\text{O}$ and obtain climatic
278 information. For this reason, the $\delta^{18}\text{O}_{\text{carb}}$ values obtained in this work were converted into $\delta^{18}\text{O}_{\text{phos}}$. To do
279 so, first, to express in VSMOW notation, the $\delta^{18}\text{O}_{\text{carb}}$ was corrected using the following correlation (Brand
280 et al., 2014; Coplen et al., 1983):

281
$$\text{(Eq.5)} \delta^{18}\text{O}_{\text{carb}} (\text{VSMOW}) = 1.0309 \times \delta^{18}\text{O}_{\text{carb}} (\text{VPDB}) + 30.91$$

282 Second, considering the relationship existent in tooth enamel between the carbonate and phosphate fraction
283 (Iacumin et al., 1996; Pellegrini et al., 2011), from a compilation of the existent bibliography of modern
284 animals measurements (Bryant et al., 1996; Pellegrini et al., 2011; Trayler and Kohn, 2017), Pederzani et
285 al. (2023) proposed the following correlation:

286
$$\text{(Eq.6)} \delta^{18}\text{O}_{\text{phos}} (\text{VSMOW}) = 0.941 \times c (\text{VSMOW}) - 7.16$$

287 Once the isotopic information is expressed in $\delta^{18}\text{O}_{\text{phos}}$ (VSMOW), we can estimate the $\delta^{18}\text{O}$ on meteoric
288 waters ($\delta^{18}\text{O}_{\text{mw}}$). It is known that different physiological factors will condition how oxygen isotope
289 composition is fixed in each mammalian group. Thus, the correlations are usually species-specific and
290 developed considering the physiology of each animal group. The obligate drinkers heavily rely on
291 consuming large amounts of liquid drinking water, being the relative contribution of water from plants
292 negligible and then minimizing the possible impact of isotopic enrichment through evapotranspiration in
293 plants (Hoppe, 2006; Maloiy, 1973, Pederzani and Britton, 2019). However, certain types of drinking
294 behaviours can impact $\delta^{18}\text{O}$, such as systematic consumption of certain highly buffered water sources
295 (rivers or lakes), can significantly attenuate the final signal recorded. The correlation employed by this
296 work relies on recent data compilations (Pederzani et al., 2021b, 2023). In the case of horses (Eq. 7), it has
297 been considered the data combination of Blumenthal et al. (2019); Chillón et al. (1994); Bryant et al., 1994;
298 Delgado Huertas et al., 1995), whereas for bovines (Eq. 8) the data from D'Angela and Longinelli (1990)
299 and Hoppe (2006) have been put together in Eq. 4. To estimate $\delta^{18}\text{O}_{\text{mw}}$ from red deer remains, we selected
300 D'Angela and Longinelli (1990) correlation (Eq. 9):

301
$$\text{(Eq.7)} \delta^{18}\text{O}_{\text{mw}} (\text{VSMOW}) = (\delta^{18}\text{O}_{\text{phos}} (\text{VSMOW}) - 22.14) / 0.62$$

302
$$\text{(Eq.8)} \delta^{18}\text{O}_{\text{mw}} (\text{VSMOW}) = (\delta^{18}\text{O}_{\text{phos}} (\text{VSMOW}) - 22.36) / 0.78$$

303
$$\text{(Eq.9)} \delta^{18}\text{O}_{\text{mw}} (\text{VSMOW}) = (\delta^{18}\text{O}_{\text{phos}} (\text{VSMOW}) - 24.39) / 0.91$$

304 Finally, paleotemperatures estimations from $\delta^{18}\text{O}_{\text{mw}}$ are typically approached using a geographically
305 adjusted linear regression, which can vary from precise adjustments (aimed at reducing errors) to broader
306 geographical adjustments that encompass more variability but are less precise (e.g., Pryor et al., 2014;
307 Skrzypek et al., 2011; Tütken et al., 2007). In this work, temperatures were calculated considering the linear
308 regression model relating $\delta^{18}\text{O}_{\text{mw}}$ and air temperatures proposed by Pederzani et al. (2021) based on
309 monthly climatic records (monthly mean $\delta^{18}\text{O}_{\text{mw}}$ and monthly mean air temperatures), from Western,
310 Southern and Central Europe stations from the Global Network of Isotopes in Precipitation (IAEA/ WMO,
311 2020). Considering current IAEA data sets from northern Iberia, there is a strong positive relationship
312 between $\delta^{18}\text{O}_{\text{mw}}$ and annual or monthly temperatures (Moreno et al., 2021). However, it is known that Iberia
313 is under a mixed influence between Atlantic and Mediterranean moisture sources that affects the isotopic
314 composition of rainfall (Araguas-Araguas and Diaz Teijeiro, 2005; García-Alix et al., 2021; Moreno et al.,
315 2021). Given uncertainties in past atmospheric circulation patterns and the limited availability of reference
316 stations, it was deemed most appropriate to select an equation that extends beyond the borders of Iberia and
317 incorporates higher variability. Different correlations were for mean annual temperature (Eq. 10), summer
318 (Eq. 11), and winter (Eq. 12) temperatures (T):

319
$$\text{(Eq.10)} \delta^{18}\text{O}_{\text{mw}} (\text{VSMOW}) = (0.50 \times T) - 13.64$$

320
$$\text{(Eq.11)} \delta^{18}\text{O}_{\text{mw}} (\text{VSMOW}) = (0.46 \times T) - 14.70$$

321
$$\text{(Eq.12)} \delta^{18}\text{O}_{\text{mw}} (\text{VSMOW}) = (0.52 \times T) - 11.26$$

322 Nonetheless, oscillations between glacial and interglacial conditions in the past have influenced global ice
323 volume and sea level fluctuations (Dansgaard, 1964; Shackleton, 1987), impacting seawater oxygen isotope
324 composition and the surface hydrological cycle on a worldwide scale, including $\delta^{18}\text{O}_{\text{mw}}$ (Schrag et al.,
325 2002). Prior studies have used sea level information to correct $\delta^{18}\text{O}_{\text{mw}}$ (e.g., Fernández-García et al., 2019;
326 Schrag et al., 2002). Given the chronological uncertainty in the studied levels, a general correction was
327 applied to $\delta^{18}\text{O}_{\text{mw}}$ before temperature estimations, following Fernández-García et al. (2020) approach.
328 Considering the mean sea level descent for the MIS 3 period (50 meters below present-day sea
329 level)(Chappell and Shackleton, 1986), this may have contributed to a potential increase in the global
330 $\delta^{18}\text{O}_{\text{mw}}$ value by $\approx 0.5\%$, inferring a bias in calculated air temperatures of $\approx 1^\circ\text{C}$.

331 Due to the uncertainties incurred from converting stable isotope measurements to palaeotemperature, the
332 final estimations in this work should be considered exploratory and as a method of standardisation to make
333 results comparable among different sites, species, and other non-isotopic palaeoclimatic records. In these
334 estimations, the associated error from converting $\delta^{18}\text{O}_{\text{phos}}$ to MAT is enlarged by the uncertainty derived
335 from the transformation of $\delta^{18}\text{O}_{\text{carb}}$ (VPDB) to $\delta^{18}\text{O}_{\text{phos}}$ (VSMOW) (see Pryor et al., 2014; Skrzypek et al.,
336 2016 for further discussion). However, Pryor et al. (2014) and Pederzani et al. (2023) concluded that the
337 impact of this conversion is negligible compared to the error propagation in subsequent calibrations used
338 for temperature estimations from $\delta^{18}\text{O}_{\text{phos}}$. These associated errors were quantified following the
339 methodology outlined by Pryor et al. (2014) (Appendix B).

340 **3.6 Inverse modelling applied to intratooth profiles**

341 Intratooth profiles frequently provide a time-averaged signal compared to the input isotopic signal ($\delta^{13}\text{C}/$
342 $\delta^{18}\text{O}_{\text{carb}}$) during enamel formation (Passey et al., 2005b). This signal attenuation is caused by time-averaging
343 effects incurred through the extended nature of amelogenesis and tooth formation, and through the sampling
344 strategy. During mineralisation, the maturation zone, which is time-averaged, often affects a large portion
345 of the crown height and might affect the temporal resolution of the input signal of the sample taken. To
346 obtain climatically informative seasonal information on the analysed teeth, the inverse modelling method
347 proposed by (Passey et al. (2005b) is applied in this work. This method computationally estimates the time-
348 averaging effects of sampling and tooth formation to obtain the original amplitude of the isotopic input
349 signal more accurately, thus, to summer and winter extremes (Appendix E). This method considers
350 parameters based on the amelogenesis trends of each species and sampling geometry, which are critical for
351 a meaningful interpretation of intratooth isotope profiles. The model also estimates the error derived from
352 the sampling uncertainty and the mass spectrometer measurements to evaluate the data's reproducibility
353 and precision. This method was initially developed for continuously growing teeth, taking into account a
354 constant growth rate within a linear maturation model, with a progressive time-average increment as
355 sampling advances along the teeth profile. The species studied in this research exhibit non-linear tooth
356 enamel formation, particularly in later-forming molars (Bendrey et al., 2015; Blumenthal et al., 2014; Kohn,
357 2004; Passey and Cerling, 2002; Zazzo et al., 2012). Although the model mentioned above is not ideal, as
358 it does not take into account non-linear enamel formation and specific growth parameters for the species
359 included are unknown, it is the best estimation based on the current state of the field and remains widely
360 used (Pederzani et al., 2021a, b, 2023). Flat and less sinusoidal profiles are less suitable for the application
361 of the model, given its inherent assumption of an approximately sinusoidal form. Therefore, we chose not
362 to apply this methodology in the analysis of intratooth $\delta^{13}\text{C}$ profiles, and it is recommended to approach the
363 interpretation of model outcomes for non-sinusoidal $\delta^{18}\text{O}$ curves with caution. Further details on the
364 application of this method can be found in Appendix E.

365 Following Pederzani et al. (2021b), mean annual temperatures (MAT) were deduced from the average of
366 $\delta^{18}\text{O}_{\text{carb}}$ values between summer and winter detected in original sinusoidal intratooth profiles (Appendix
367 D). This work shows that comparable results for annual means can be obtained before and after model
368 application, but doing it beforehand avoids the associated errors induced by the inverse model. To maximize
369 data, in non-sinusoidal teeth profiles, MAT was deduced from the average of all points within a tooth.
370 However, this approach is less reliable when complete annual cycles are not recorded. When possible,

371 summer and winter temperature estimations were derived from the obtained $\delta^{18}\text{O}_{\text{carb}}$ values after inverse
372 modelling application, aiming to identify the corrected seasonal amplitude, which is dampened in the
373 original $\delta^{18}\text{O}_{\text{carb}}$ signal.

374 **3.7 Present-day isotopic and climatic data**

375 Present-day climatic conditions surrounding each site have been considered, allowing an inter-site
376 comparison, essential for compare this study with other regional and global data. Considering current MATs
377 and MAPs, estimated climatic data is expressed in relative terms as MAT and MAP anomalies. Present-
378 day summer and winter temperatures were also considered. Present-day temperatures and precipitation
379 values were obtained from the WorldClim Dataset v2 (Fick and Hijmans, 2017) (Appendix B). This dataset
380 includes the average of bioclimatic variables between 1970-2000 in a set of raster files with a spatial
381 resolution every 2.5 minutes. The exact location of the selected archeo-palaeontological sites was used,
382 using geographical coordinates in the projection on modern climatic maps with QGIS software.

383 Present-day $\delta^{18}\text{O}_{\text{mw}}$ values from the analysed sites' areas were obtained using the Online Isotopes in
384 Precipitation Calculator (OIPC Version 3.1 (4/2017); Bowen, 2022) based on datasets collected by the
385 Global Network for Isotopes in Precipitation from the IAEA/WMO (Appendix B).

386

Site	Level	Culture	Species	Tooth type	Code	C	C	δ^{13}	m	m	S	Range	δ^{18}	m	m	S	Range
						E	E	Cca	in	a	D	e	Oca	in	a	D	e
						(((x			(x		
						%)	%)	VP					VP				
))	DB					DB				
								(‰)					(‰)				
Axlor	III	Mousterian	<i>Bos/Bison</i> sp.	LRM3	AX L59	5.6	1.4	-8.9	9.6	8.2	1.4	0.4	-6.0	7.3	5.2	7.7	2.1
Axlor	III	Mousterian	<i>Bos/Bison</i> sp.	LRM2	AX L60	5.5	1.8	-9.7	0.1	8.9	1.1	0.3	-5.7	6.8	4.6	7.7	2.2
Axlor	III	Mousterian	<i>Bos/Bison</i> sp.	LRM3	AX L65	6.2	1.3	-8.9	9.3	8.1	2.0	0.4	-6.0	7.2	4.8	8.8	2.6
Axlor	III	Mousterian	<i>Bos/Bison</i> sp.	LRM2	AX L66	5.6	1.6	-8.9	9.8	8.3	5.0	0.5	-4.8	6.1	3.8	7.7	2.3
Axlor	IV	Mousterian	<i>Bos/Bison</i> sp.	LRM2	AX L70	5.7	1.2	-9.1	9.4	8.6	7.0	0.3	-5.3	7.3	3.9	2.3	3.4
Axlor	VI	Mousterian	<i>Bos/Bison</i> sp.	LLM3	AX L77	5.9	1.4	-9.7	0.2	9.2	0.0	0.4	-6.2	7.9	5.0	9.9	2.9
Axlor	VI	Mousterian	<i>Bos/Bison</i> sp.	LLM3	AX L86	5.5	1.8	-9.9	0.2	9.3	9.0	0.3	-5.4	6.5	3.8	7.7	2.6
El Castillo	20E	Mousterian	<i>Equus</i> sp.	LRP3/LRP4	CA S60	1.4	-	11.9	2.5	1.5	0.0	0.3	-3.3	4.1	4.4	4.4	1.6
El Castillo	20E	Mousterian	<i>Equus</i> sp.	LRP3/LRP4	CA S61	1.4	-	12.2	4.4	1.3	3.0	0.1	-4.9	8.8	3.4	4.1	1.5
El Castillo	20E	Mousterian	<i>Bos/Bison</i> sp.	LLM2	CA S13	6.9	1.6	-	2.2	1.9	9.0	0.3	-5.6	3.3	9.5	5.1	1.4
El Castillo	20E	Mousterian	<i>Bos/Bison</i> sp.	LLM2	CA S14	5.0	1.7	-	1.9	1.8	8.0	0.3	-5.5	3.3	6.6	6.1	1.7
El Castillo	21A	Mousterian	<i>Bos/Bison</i> sp.	LLM3	CA S14	5.1	1.5	-	1.5	0.9	6.0	0.2	-5.4	5.5	3.6	6.2	2.2
El Castillo	21A	Mousterian	<i>Bison</i> <i>priscus</i>	LLM3	CA S14	6.2	1.5	-	1.7	0.9	7.0	0.2	-5.0	7.4	4.4	4.1	1.3
El Castillo	21A	Mousterian	<i>Equus</i> sp.	LLM3	CA S14	6.3	1.7	-	2.9	2.4	4.0	0.1	-6.2	2.2	4.5	5.1	1.8

		Transitiona							-	-							
		l			CA				1	1	0			-	-	0	
El	18	Aurignacia	<i>Bos/Bison</i>	S13	6.	1	-	1.	0.	.				7.	4.	.	
Castillo	B	n	on sp.	ULM2	2	2	3	11.3	5	9	6	0.2	-6.2	4	9	7	2.6
		Transitiona							-	-							
		l			CA				1	1	1			-	-	0	
El	18	Aurignacia	<i>Bos/Bison</i>	S13	6.	1	-	1.	0.	.				6.	4.	.	
Castillo	B	n	on sp.	ULM2	3	8	8	10.9	6	5	1	0.3	-5.4	5	2	7	2.2
		Transitiona							-	-							
		l			CA				1	1	1			-	-	0	
El	18	Aurignacia	<i>Bos/Bison</i>	S13	6.	1	-	2.	1.	.				6.	4.	.	
Castillo	B	n	on sp.	ULM2	4	6	8	12.4	8	6	2	0.3	-5.4	3	5	5	1.8
		Transitiona							-	-							
		l			CA				1	1	0			-	-	0	
El	18	Aurignacia	<i>Bos/Bison</i>	S13					1.	1.	.			6.	5.	.	
Castillo	C	n	on sp.	LLM3	5	6	7	11.3	5	0	5	0.2	-6.1	6	5	3	1.1
		Transitiona							-	-							
		l			CA				1	1	0			-	-	0	
El	18	Aurignacia	<i>Bos/Bison</i>	S13	5.	1	-	2.	1.	.				6.	5.	.	
Castillo	C	n	on sp.	LLM3	6	8	7	12.0	5	7	9	0.2	-5.8	7	0	6	1.7
		Transitiona							-	-							
		l			CA				1	-	0			-	-	0	
El	18	Aurignacia	<i>Bos/Bison</i>	S13	6.	1	-	0.	9.	.				6.	4.	.	
Castillo	C	n	on sp.	LLM3	7	6	4	10.2	6	9	7	0.2	-5.8	5	1	7	2.4
		Transitiona							-	-							
		l			CA				1	1	0			-	-	0	
El	18	Aurignacia	<i>Bos/Bison</i>	S13	6.	1	-	1.	1.	.				5.	4.	.	
Castillo	C	n	on sp.	LLM3	8	1	8	11.6	8	4	4	0.1	-5.3	9	8	3	1.2
		Transitiona							-	-							
		l		ULM2					1	1	2			1	-	2	
El	18	Aurignacia	<i>Cervus elaphus</i>	+ULM	CA				1	-	4.	2.	.	0.	4.	.	
Castillo	B	n		3	S8	1	13.0	9	1	8	1.0	-6.8	4	1	1	6.3	
		Transitiona							-	-							
		l							1	1	0			-	-	0	
El	18	Aurignacia	<i>Equus</i>	ULP3/	CA				1.	1.	.			7.	5.	.	
Castillo	B	n	sp.	ULP4	S58	9	11.7	8	5	3	0.1	-6.6	5	6	5	1.8	
		Transitiona							-	-							
		l							1	1	0			-	-	0	
El	18	Aurignacia	<i>Equus</i>	LLP3/	CA				1.	1.	.			4.	3.	.	
Castillo	B	n	sp.	LLP3	S59	4	11.5	7	0	7	0.2	-4.0	7	5	4	1.2	
									-	-							
					LA				1	1	0			-	-	0	
Labeko	IX	Chatelperro	<i>Equus</i>		B3				1	-	2.	1.	.	7.	5.	.	
Koba	inf	nian	sp.	URM3	8	7	12.0	2	9	3	0.1	-6.6	7	9	5	1.9	
									-	-							
					LA				1	1	0			-	-	1	
Labeko	IX	Chatelperro	<i>Cervus elaphus</i>		B0				-	2.	2.	.		6.	3.	.	
Koba	inf	nian		LLM2	2	7	12.3	4	1	3	0.1	-4.7	0	7	0	2.3	
									-	-							
					LA				1	1	0			-	-	0	
Labeko		Aurignacia	<i>Equus</i>		B2				1	-	2.	1.	.	6.	4.	.	
Koba	VI	n	sp.	URM2	0	6	12.0	2	8	4	0.1	-5.3	1	4	6	1.7	
									-	-							
					LA				1	1	0			-	-	0	
Labeko		Aurignacia	<i>Equus</i>		B4				1	-	2.	1.	.	6.	5.	.	
Koba	V	n	sp.	LRM3	2	7	11.9	3	5	2	0.7	-5.7	6	0	5	1.6	
														-	-	0	
Labeko		Aurignacia	<i>Equus</i>		B3				1	-	-	.		6.	5.	.	
Koba	IV	n	sp.	LRM2	6	7	11.6	1	1	6	0.2	-5.9	2	5	2	0.7	

																			1.	1.
																			8	3
																			-	-
				CA															1	-
				N0	7.	1	-	0.	9.	.									-	0
Canyars	I	Aurignacia	<i>Equus</i>	URM3	1	8	2	10.0	4	5	9	0.3	-4.8	3	3	3	3	1.1	-	-
			sp.																-	0
				CA															1	1
				N0	6.	1	-	0.	0.	.									-	0
Canyars	I	Aurignacia	<i>Equus</i>	URM3	2	2	7	10.5	7	3	4	0.1	-4.4	0	6	5	1.4		-	-
			<i>ferus</i>																-	0
				CA															1	1
				N0	6.	1	-	1.	0.	.									-	0
Canyars	I	Aurignacia	<i>Equus</i>	URP3/	3	4	7	10.7	2	4	8	0.2	-4.8	3	0	4	1.4		-	-
			<i>ferus</i>	URP4															-	0
				LA															1	-
			<i>Bos</i>																-	0
			<i>primigenius</i>	LRM3	3	2	3	-9.5	1	7	4	0.3	-5.7	0	2	9	2.8		-	-
Labeko Koba	VI	Aurignacia																	1	-
	I			B5	5.	2	-	0.	8.	.									-	-
				LRM3															1	-
			<i>Bos</i>																-	-
			<i>primigenius</i>	LRM3	5	6	3	10.4	5	8	6	0.3	-5.1	0	7	2	4.3		-	-
Labeko Koba	VI	Aurignacia																	1	-
	I			B5	5.	2	-	1.	9.	.									-	-
				LRM3															1	-
			<i>Bos/Bison</i>																1	-
			sp.	LRM3	2	5	1	-9.7	2	1	2	0.3	-7.2	1	2	6	2.0		-	-
Labeko Koba	VI	Aurignacia																	1	-
	I			B6	6.	2	-	0.	9.	.									-	-
				LRM3															1	-
			<i>Bos</i>																1	-
			<i>primigenius</i>	LRM3	9	5	1	-9.3	3	3	0	0.9	-7.2	8	5	9	3.3		-	-
Labeko Koba	V	Aurignacia																	1	-
				B6	5.	2	-	0.	7.	.									-	-
				LRM3															1	-
			<i>Bos</i>																1	-
			<i>primigenius</i>	ULM3	4	8	4	-9.3	8	7	1	0.3	-3.6	2	6	5	1.6		-	-
Canyars	I	Aurignacia																	-	-
				N0	6.	1	-	9.	8.	.									-	-
				ULM3															-	-
			<i>Bos</i>																-	-
			<i>primigenius</i>	ULM3	5	6	4	-9.0	5	5	9	0.3	-5.5	2	0	4	1.2		-	-
Canyars	I	Aurignacia																	-	-
				N0	6.	1	-	9.	8.	.									-	-
				ULM3															-	-
			<i>Bos/Bison</i>																-	-
			sp.	LLM3	0	5	7	-9.2	6	7	9	0.3	-5.5	5	3	5	2.2		-	-
Aitzbitarte III	V	Gravettian																	-	-
				AI															-	-
				TII	5.	1	-	9.	8.	.									-	-
				LLM3															-	-
			<i>Bos/Bison</i>																-	-
			sp.	LLM3	0	5	7	-9.2	6	7	9	0.3	-5.5	5	3	5	2.2		-	-
				LLM2															-	-
				+LLM															1	1
				OT	1	-	-	1.	1.	.									-	-
El Otero	IV	Magdalena	<i>Cervus</i>	OT	1	-	-	1.	1.	.									5.	2.
		n	<i>elaphus</i>	E1	1	11.4	6	2	4	0.1	-4.4	8	9	0	2.9				-	-
																			-	-
				LLM2															1	1
				+LLM															-	-
				OT	1	-	-	1.	1.	.									-	-
El Otero	IV	Magdalena	<i>Cervus</i>	OT	1	-	-	1.	1.	.									5.	3.
		n	<i>elaphus</i>	E5	0	11.3	5	0	5	0.2	-5.1	7	8	6	1.9				-	-
																			-	-
				LLM2															1	1
				+LLM															-	-
				OT	1	-	-	1.	0.	.									-	-
El Otero	IV	Magdalena	<i>Cervus</i>	OT	1	-	-	1.	0.	.									5.	4.
		n	<i>elaphus</i>	E6	4	11.4	8	6	2	0.3	-4.6	4	0	4	1.4				-	-
																			-	-
				LLM2															1	1
				+LLM															-	-
				OT	1	-	-	1.	1.	.									-	-
El Otero	IV	Magdalena	<i>Equus</i>	OT	1	-	-	1.	1.	.									-	-
		n	sp.	LLP3/	7	11.6	8	4	5	0.1	-5.0	3	9	7	2.4				-	-
				LLP4															-	-
				E11															-	-
																			-	-
				LLM2															1	1
				+LLM															-	-
				OT	1	-	-	1.	0.	.									-	-
El Otero	IV	Magdalena	<i>Equus</i>	OT	1	-	-	1.	0.	.									-	-
		n	sp.	LLP3/	6	11.3	5	9	6	0.1	-3.9	9	3	6	1.6				-	-
				LLP4															-	-
				E12															-	-

387 **Table 2.** Mean, maximum value (Max), minimum value (Min), and standard deviation (SD) of $\delta^{13}\text{C}$ and
 388 $\delta^{18}\text{O}$ values per archaeological site and level organised by cultural periods. CCE, calcium carbonate
 389 equivalent; n, number of intratooth subsamples measured. In tooth type: position (U, upper; L, lower);
 390 laterality (R, right; L, left); tooth (M, molar; P, premolar).

391

392 4. Results

393 In northwestern Iberia, specifically in the Vasco-Cantabrian region, the mean $\delta^{13}\text{C}_{\text{carb}}$ values range from -
 394 13‰ to -8.9‰, with a mean value of -11‰ (SD = 1.2‰) (Table 2; Table 3). Considering species' different
 395 enrichment factors, the $\delta^{13}\text{C}_{\text{carb}}$ were transformed in $\delta^{13}\text{C}_{\text{diet}}$, resulting in mean values that extend from -
 396 27‰ to -23.5‰ (Fig. 4). It must be considered that average values may reflect slightly different periods or
 397 be affected by seasonal bias because different teeth encompass diverse periods, but it has been verified in
 398 our teeth that the variations are limited when the seasonal information of the sequential sampling is
 399 incorporated (± 0.2 ; Appendix B). The carbon isotopic composition varies between species. The bovines
 400 have generally higher mean $\delta^{13}\text{C}_{\text{carb}}$ (from -12.4‰ to -8.9‰) than the horses (from -12.6‰ to -11.3‰),
 401 whereas the red deer fall within the horses' range (from -13‰ to -11.3‰). Average values of $\delta^{18}\text{O}_{\text{carb}}$ in all
 402 Vasco-Cantabrian individuals extend between -7.2‰ and -3.3‰ (mean = -5.5‰; SD = 0.8‰). When
 403 transformed to $\delta^{18}\text{O}$ expected from meteoric waters ($\delta^{18}\text{O}_{\text{mw}}$), with species-adapted correlations, the $\delta^{18}\text{O}_{\text{mw}}$
 404 values range from -10.6‰ to -5.5‰. Less clear patterns in $\delta^{18}\text{O}_{\text{carb}}$ are observed between bovines and
 405 horses, with mean values of -5.7‰ and -5.2‰, respectively. In northeastern Iberia, the site of Canyars, both
 406 species have relatively high $\delta^{18}\text{O}_{\text{carb}}$ values that fall inside the range of variation observed in the Cantabria
 407 region, between -5.5‰ and -3.6‰ in bovines and between -4.8‰ and -4.4‰ in horses.

408

		Vasco-Cantabrian region (NW Iberia)				Northeastern Iberia			
		$\delta^{13}\text{C}_{\text{carb}}$ VPDB (‰)	$\delta^{13}\text{C}_{\text{diet}}$ VPDB (‰)	$\delta^{18}\text{O}_{\text{carb}}$ VPDB (‰)	$\delta^{18}\text{O}_{\text{mw}}$ VSMOW (‰)	$\delta^{13}\text{C}_{\text{carb}}$ VPDB (‰)	$\delta^{13}\text{C}_{\text{diet}}$ VPDB (‰)	$\delta^{18}\text{O}_{\text{carb}}$ VPDB (‰)	$\delta^{18}\text{O}_{\text{mw}}$ VSMOW (‰)
Total	Mean	-11.0	-25.1	-5.5	-8.0	-9.9	-24.0	-4.6	-7.1
	Max	-8.9	-23.5	-3.3	-5.5	-9.0	-23.6	-3.6	-5.0
	Min	-13.0	-27.0	-7.2	-10.6	-10.7	-24.4	-5.5	-7.9
	Range	4.1	3.5	3.9	5.1	1.7	0.8	1.9	2.9
	SD	1.2	0.9	0.8	1.2	0.8	0.3	0.7	1.2
Bovines	Mean	-10.4	-25.0	-5.7	-7.7	-9.1	-23.7	-4.5	-6.2
	Max	-8.9	-23.5	-4.8	-6.5	-9.0	-23.6	-3.6	-5.0
	Min	-12.4	-27.0	-7.2	-9.5	-9.3	-23.9	-5.5	-7.4
	Range	3.5	3.5	2.4	3.0	0.3	0.3	1.9	2.4
	SD	1.1	1.1	0.6	0.7	0.2	0.2	1.4	1.7
Horses	Mean	-11.8	-25.5	-5.2	-8.5	-10.4	-24.1	-4.7	-7.6
	Max	-11.3	-25.0	-3.3	-5.5	-10.0	-23.7	-4.4	-7.2
	Min	-12.6	-26.3	-6.6	-10.6	-10.7	-24.4	-4.8	-7.9
	Range	1.4	1.4	3.3	5.1	0.7	0.7	0.5	0.7
	SD	0.4	0.4	1.1	1.8	0.3	0.3	0.3	0.4

409

410 **Table 3.** Mean $\delta^{13}\text{C}$ from enamel carbonate ($\delta^{13}\text{C}_{\text{carb}}$) and diet ($\delta^{13}\text{C}_{\text{diet}}$), and $\delta^{18}\text{O}$ from enamel carbonate
411 ($\delta^{18}\text{O}_{\text{carb}}$) and meteoric waters ($\delta^{18}\text{O}_{\text{mw}}$), by species on the Vasco-Cantabrian and northeastern Iberia areas.
412 Max: maximum value; Min: minimum value; SD: standard deviation.

413 **4.1 Axlor (Mousterian, ca. 80 ka BP - 50 ka cal BP)**

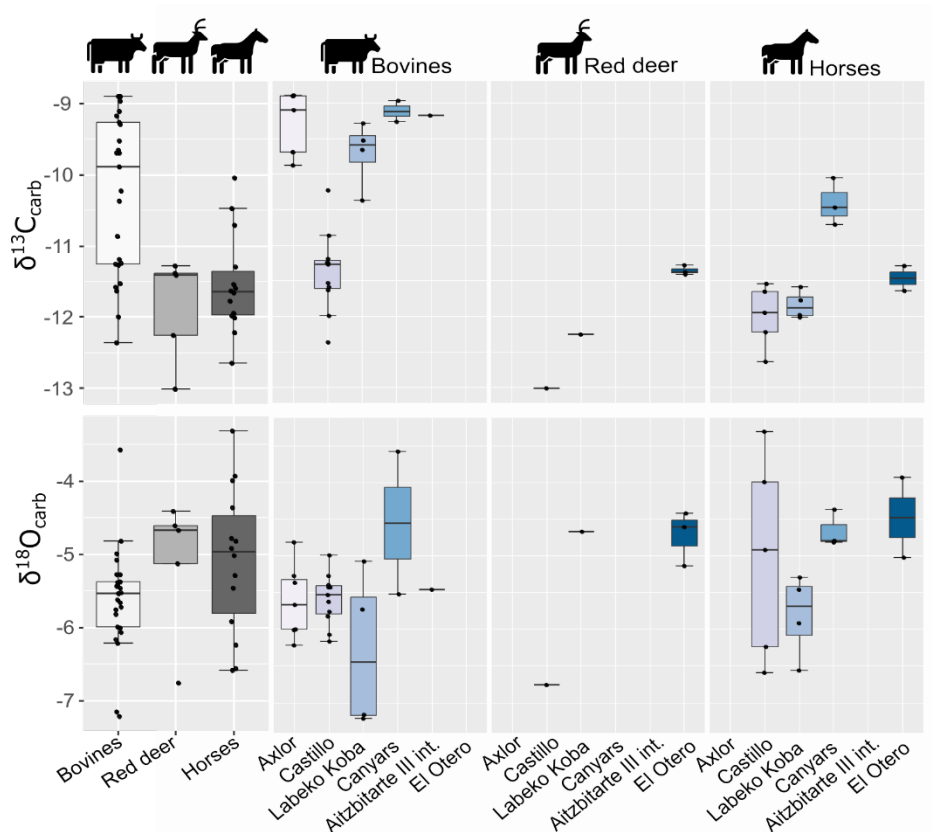
414 A total of seven bovine teeth were included from levels III (n = 4), IV (n = 1), and VI (n = 2) of Axlor cave
415 (Pederzani et al., 2023). The mean $\delta^{13}\text{C}_{\text{carb}}$ range from -9.9‰ to -8.9‰ ($\delta^{13}\text{C}_{\text{diet}}$ = -24.5‰ to -23.5‰);
416 whereas mean $\delta^{18}\text{O}_{\text{carb}}$ values are between -6.2‰ and -4.8‰ ($\delta^{18}\text{O}_{\text{mw}}$ = -8.3‰ and -6.5‰), indicating a
417 range of variation around 1‰ and 1.4‰, respectively (Fig. 3; 4). Considering isotopic compositions by
418 levels, mean $\delta^{13}\text{C}_{\text{carb}}$ decreases from level III to level IV, whereas mean $\delta^{18}\text{O}_{\text{carb}}$ remains stable through the
419 sequence (Table 2; Appendix B). A range between 0.3‰ and 0.5‰ is observed in $\delta^{13}\text{C}_{\text{carb}}$ variation within
420 tooth profiles. Individuals show clear $\delta^{18}\text{O}$ sinusoidal profiles, with peaks and troughs and intratooth ranges
421 from 2.1‰ to 3.4‰. The $\delta^{18}\text{O}_{\text{mw}}$ after inverse modelling intratooth profiles range from -9.1‰ to -7.35‰
422 (Appendix D; E). Mean Annual Temperatures (MATs) oscillated between 9.1°C and 12.6°C (MATAs = -
423 3.1/+0.4°C) (Table 4). From sinusoidal profiles, summer temperatures were extracted from peaks, resulting
424 from 15.4°C to 23.7°C, and winter temperatures from troughs provided values ranging from -7°C to 10.8°C.
425 Mean Annual Precipitation (MAPs), extracted from $\delta^{13}\text{C}_{\text{carb}}$, extend between 204mm and 326mm (MAPAs
426 = -843/-721mm). Based on these estimations, a non-clear climatic trend is observed through these levels.

427 **4.2 El Castillo (Mousterian and Transitional Aurignacian, 62.5 ka BP – 46.4 ka cal BP)**

428

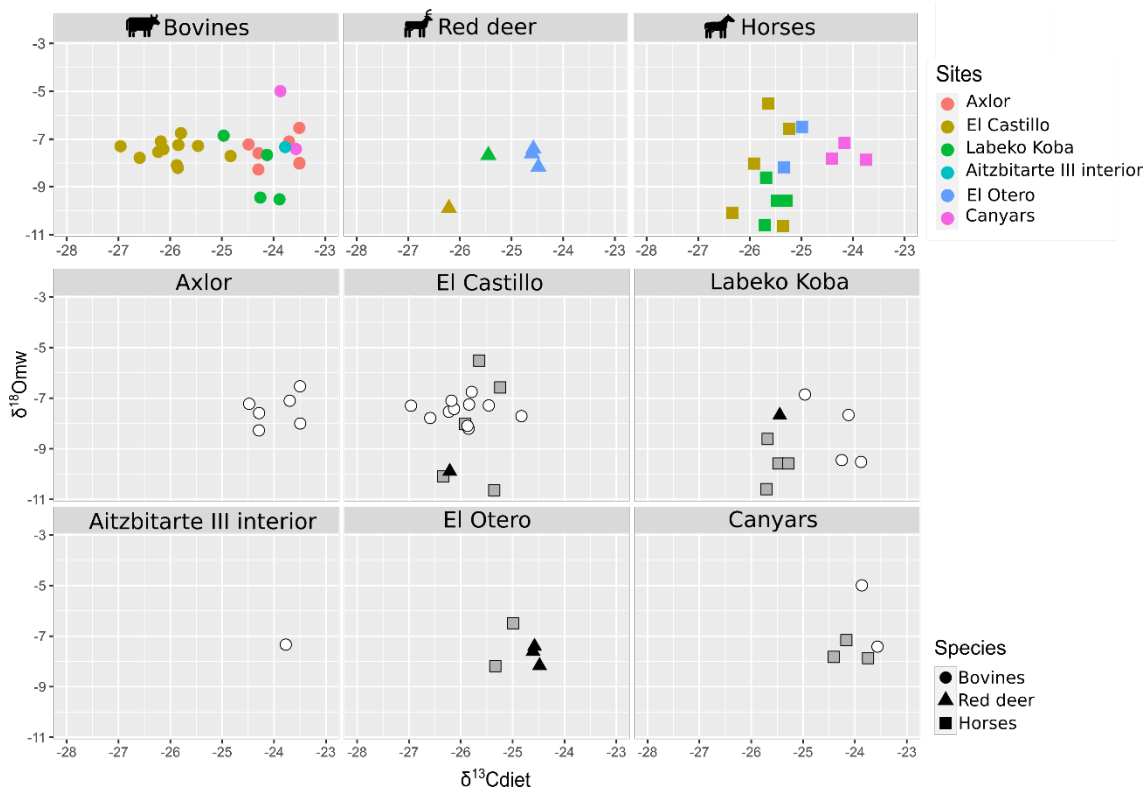
429 From El Castillo, this work includes bovines (n = 11), horses (n = 5), and red deer (n = 1) teeth from the
430 Mousterian (21 and 20E) and the Transitional Aurignacian levels (18B and 18C). The mean $\delta^{13}\text{C}_{\text{carb}}$ values
431 are lower for horses, bovines, and red deer (-13‰ to -10.2‰) than other sites. Between -12.4‰ and -10.2‰
432 for bovines ($\delta^{13}\text{C}_{\text{diet}}$ = -24.6‰ to -25.8‰) and between -12.6‰ and -11.5‰ for horses ($\delta^{13}\text{C}_{\text{diet}}$ = -26.3‰
433 to -25.2‰) (Fig. 3). The mean $\delta^{18}\text{O}_{\text{carb}}$ values extend from -6.8‰ and -3.3‰. Horses and bovines overlap
434 in their isotopic niche (Fig. 4), mainly due to the notably lower $\delta^{13}\text{C}_{\text{carb}}$ reported by bovines. The mean
435 $\delta^{13}\text{C}_{\text{carb}}$ (-13‰) of the single red deer tooth is inside the variation range of bovines and horses but with a
436 lower $\delta^{18}\text{O}_{\text{carb}}$ mean value (-6.8‰). Considering these isotopic compositions by levels, bovine mean $\delta^{13}\text{C}_{\text{diet}}$
437 values highly increase the variation range from Mousterian levels (20E and 21A) to Transitional
438 Aurignacian levels (18C and 18B). In contrast, horses increase mean $\delta^{13}\text{C}_{\text{diet}}$ values (Fig. 5). Bovine mean
439 $\delta^{18}\text{O}_{\text{mw}}$ values decrease from level 21A to level 18B, while horses from 18B have a large intra-level
440 amplitude.

441 The mean $\delta^{18}\text{O}_{\text{carb}}$ values from horses have a more significant variation (range = 3.3‰) than bovines (range
442 = 2.2‰). All individuals show flat $\delta^{13}\text{C}_{\text{carb}}$ intratooth profiles (<0.4‰), except for red deer (1‰) (Appendix
443 D). Intratooth $\delta^{18}\text{O}_{\text{carb}}$ ranges of individuals are around 1-2‰ for horses and 1-3‰ for bovines. Some of
444 the individuals analyzed do not show non-complete annual cycles. No precise $\delta^{18}\text{O}_{\text{carb}}$ sinusoidal profiles
445 are detected in three teeth; the other six have particularly unclear profiles. After modelling, individual
446 $\delta^{18}\text{O}_{\text{carb}}$ ranges oscillated between 2.7‰ and 7.4‰ (Appendix E). MATs oscillated between 4.6°C and
447 12.6°C (MATAs = -8.8°C/-0.9°C), with mean summer temperatures from around 20.5°C and mean winter
448 temperatures around -1.1°C. MAPs extend between 376mm and 784mm (MAPAs = -656/-248mm) (Table
449 4). Non-important differences in rainfall estimations based on bovines and equids are noticed, probably
450 because they feed on similar ecological resources. Diachronic trends are unclear along the sequence but
451 mean annual and winter temperatures from levels 18C and 18C seem slightly lower. MAPs estimations
452 oscillated more in the upper levels.



453

454 **Figure 3.** Distribution of mean carbon ($\delta^{13}\text{C}_{\text{carb}}$) and oxygen ($\delta^{18}\text{O}_{\text{carb}}$) isotopic values of enamel carbonate
 455 by species and archaeological site.



456

457

458

Figure 4. Biplot crossing $\delta^{13}\text{C}$ from diet ($\delta^{13}\text{C}_{\text{diet}}$) and $\delta^{18}\text{O}$ from meteoric waters ($\delta^{18}\text{O}_{\text{mw}}$) by species and archaeological site.

459 **4.3 Labeko Koba (Châtelperronian and Aurignacian, 45.1-36.3 ka cal BP)**

460 This work includes bovines (n = 4), horses (n = 4), and red deer (n = 1) teeth from levels related to
461 Châtelperronian (IXb inf), ProtoAurignacian (VII), and Aurignacian (VI, V, and IV). Significant
462 differentiation in mean $\delta^{13}\text{C}_{\text{carb}}$ between bovines and horses is observed, with higher values between -9.3‰
463 and -10.4‰ in bovines ($\delta^{13}\text{C}_{\text{diet}} = -25\text{‰}$ to -23.8‰) than equids, whose values extend from -12‰ to -11.6‰
464 ($\delta^{13}\text{C}_{\text{diet}} = -25.8\text{‰}$ to -25.2‰) (Fig. 3;). These horses' values are within the ranges observed from this
465 species in the region. Red deer have similar $\delta^{13}\text{C}_{\text{carb}}$ values to those of horses ($\delta^{13}\text{C}_{\text{carb}} = -12.3\text{‰}$; $\delta^{13}\text{C}_{\text{diet}} =$
466 -25.5‰). Mean $\delta^{18}\text{O}_{\text{carb}}$ values are similar between species from -7.2‰ to -4.7‰ ($\delta^{18}\text{O}_{\text{mw}} = -8.5\text{‰}$ to -
467 6.1‰). However, bovines have a very high variation within mean $\delta^{18}\text{O}_{\text{carb}}$ values (2.1‰), also reflected in
468 the intratooth profiles. These $\delta^{18}\text{O}$ values are lower than in other Vasco-Cantabrian sites, especially for two
469 individuals in levels VII and V (Table 3). Differences in $\delta^{13}\text{C}_{\text{diet}}$ values between bovines and horses result
470 in isotopic niche differentiation between both species (Fig. 4). The red deer niche is placed within the
471 horses' niche. The evolution of niche over time cannot be evaluated by levels due to the limited sample.
472 Considering the isotopic compositions by levels (Fig. 5), both bovines and horses experienced a slight
473 increase in mean $\delta^{13}\text{C}_{\text{diet}}$ from levels IX inf to IV, from Châtelperronian to Aurignacian. Mean $\delta^{18}\text{O}_{\text{mw}}$
474 values of bovines decrease from VII to V, whereas horses increase from IXb inf to VI to decrease from VI
475 to IV.

476 Variability of $\delta^{13}\text{C}_{\text{carb}}$ values in intratooth profiles is slightly higher (0.1-0.7‰), especially in bovines (0.3-
477 0.9‰), with more oscillating profiles than generally flat profiles observed in horses and red deer (Appendix
478 D; E). Intratooth profiles ranges of $\delta^{18}\text{O}_{\text{carb}}$ are also larger within bovines (2-4‰) than in horses (1-2‰).
479 Inverse-modelled individual $\delta^{18}\text{O}_{\text{carb}}$ ranges oscillated between 5-8‰ and 2-4‰, respectively. Sinusoidal
480 curves are observed in horses and bovines, but bovine profiles are noisier. The red deer has an extensive
481 $\delta^{18}\text{O}_{\text{carb}}$ range (6.3‰) from summer peak to an incomplete winter trough. We detect an inverse relation
482 between $\delta^{13}\text{C}_{\text{carb}}$ and $\delta^{18}\text{O}_{\text{carb}}$ in some points of these individual profiles. MATs oscillated between 5.2°C
483 and 11.4°C (MATAs = -5.6/+1.1°C), with summer temperatures from 14.5°C to 27.3°C and winter
484 temperatures from 1.9°C to -4.9°C. MAPs extend between 248mm and 521mm, notably drier than nowadays
485 (MAPAs = -798/-525mm) (Table 4). Lower rainfall levels and higher seasonal amplitudes are recorded
486 along the sequence, especially in samples from the ProtoAurignacian level VII. Relevant differences are
487 noticed between MAPs estimated from bovines and equids, the first providing more arid conditions.

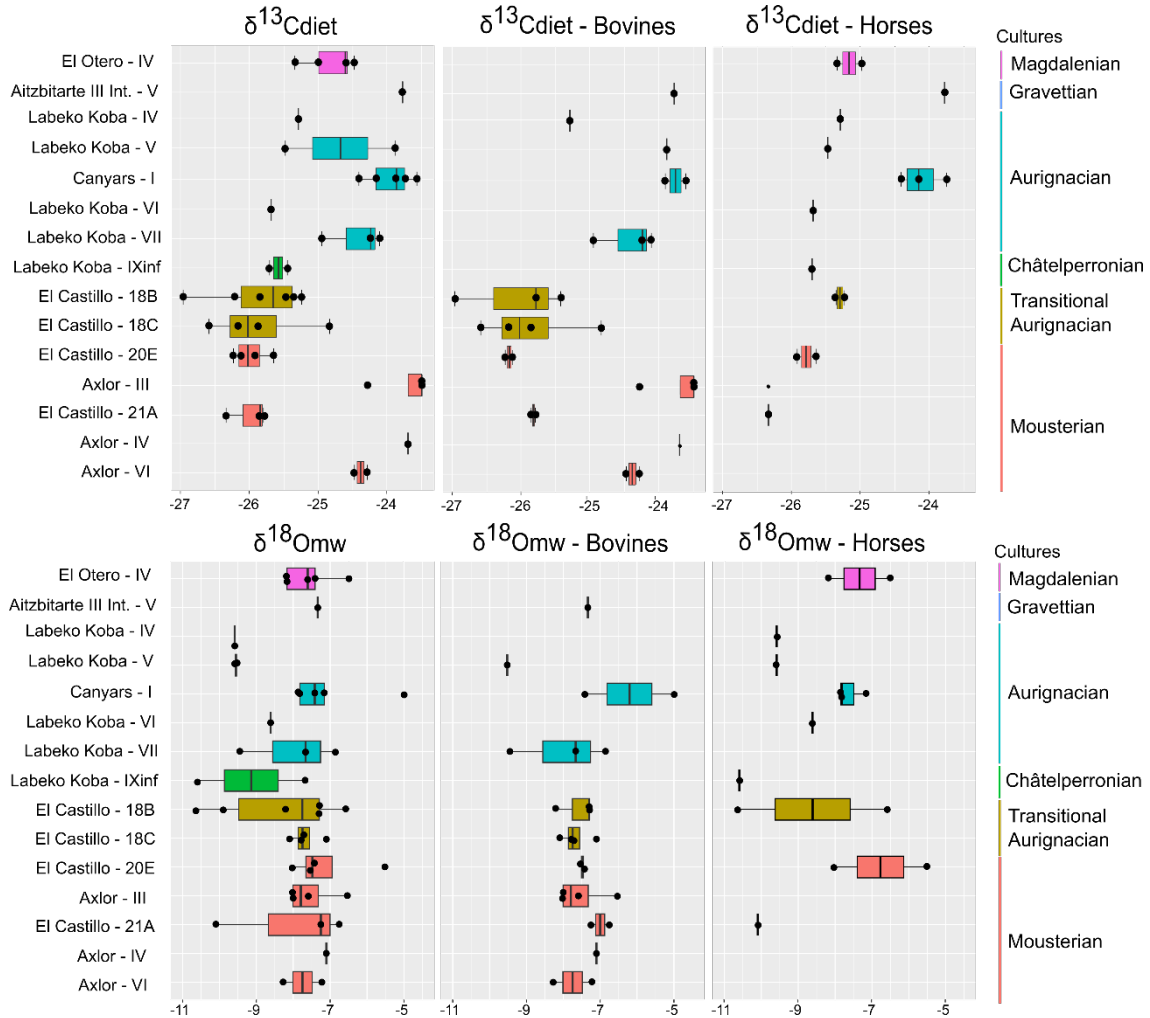
488 **4.4 Aitzbitarte III interior (Gravettian, 27.9 ka cal BP)**

489 A single bovine individual was analysed from Gravettian level V located in the inner part of the cave. It
490 has a high mean $\delta^{13}\text{C}_{\text{carb}}$ (-9.2‰) considering the observed range in bovines from the Vasco-Cantabrian
491 region, whereas the $\delta^{18}\text{O}_{\text{carb}}$ mean value (-5.5‰) is inside the common $\delta^{18}\text{O}_{\text{carb}}$ variation observed (Fig. 3).
492 The mean $\delta^{13}\text{C}_{\text{diet}}$ value of -23.8‰ is comparable with Canyars and some individuals from Axlor but
493 different from Labeko Koba and El Castillo individuals. The individual $\delta^{13}\text{C}_{\text{carb}}$ fluctuation is slight
494 (0.3‰) (Appendix D; E). These teeth show not quite sinusoidal profile shape in $\delta^{18}\text{O}_{\text{carb}}$, with an intratooth
495 range of around 2.2‰. Climatic information is extracted but may be considered cautiously due to the profile
496 shape and the limited sample size. From the inverse modelled mean $\delta^{18}\text{O}_{\text{mw}}$ value (-5.4‰), we estimate a
497 MAT of 13°C (MATA = -0.4°C) with a summer temperature of 19.7°C and winter temperature of -2.9°C.
498 The MAP estimation reached 235mm (-1127mm to nowadays) (Table 4).

499 **4.5 El Otero (Magdalenian, ca. 17.3 ka cal BP)**

500 Two equids and three cervids are included from level IV from El Otero, recently redated and chronologically
501 related to the Magdalenian (Marín-Arroyo et al., 2018). The mean $\delta^{13}\text{C}_{\text{carb}}$ values are close, between -11.4‰
502 and -11.3‰ for red deer ($\delta^{13}\text{C}_{\text{diet}} = -24.4\text{‰}$ and -24.6‰) and -11.6‰ and -11.3‰ for horse ($\delta^{13}\text{C}_{\text{diet}} = -$
503 25.3‰ and -25.3‰) (Fig. 3). These $\delta^{13}\text{C}$ values for both species are relatively high concerning other studied
504 samples, especially for cervids (around +1-2‰). Both species have higher $\delta^{18}\text{O}_{\text{carb}}$ values concerning the
505 common range of variation observed in the Vasco-Cantabria region, between -5‰ and -3.9‰ for horses
506 and between -5.1‰ and -4.4‰ for red deer. When values are transformed to $\delta^{13}\text{C}_{\text{diet}}$ and $\delta^{18}\text{O}_{\text{mw}}$, equids
507 and cervids isotopic niches are separated (Fig. 4). All individuals show low amplitude $\delta^{13}\text{C}_{\text{carb}}$ intratooth

508 profiles (<0.3‰), but especially equids with an intratooth variation around 0.1‰ (Appendix D; E). Equids
 509 and cervids show $\delta^{18}\text{O}_{\text{carb}}$ sinusoidal profiles, with intratooth ranges between 1.4‰ and 2.4‰. Climatic
 510 estimations are proposed only for equids, providing MATs estimations from 8.8°C to 12.6°C (MATAs = -
 511 4.9/-1°C) and MAP between 400mm and 456mm (MAPAs = -755/-699mm) (Table 4). A high-temperature
 512 seasonality can be seen, with summer temperatures between 19.7°C and 23.8°C and winter temperatures
 513 from -10.4°C to -3.1°C.



514
 515 **Figure 5.** Evolution of $\delta^{13}\text{C}$ in diet ($\delta^{13}\text{C}_{\text{diet}}$) and $\delta^{18}\text{O}$ in meteoric waters ($\delta^{18}\text{O}_{\text{mw}}$) by archaeological levels
 516 in a diachronic order. From right to left: all species, including cervids, bovines and horses. Colours
 517 correspond to different chrono-cultures.

518

519 4.6 Canyars (Aurignacian, 39.7 ka cal BP)

520 From the archaeological level I at Canyars, corresponding to the Aurignacian, this work includes bovines
 521 ($n = 2$) and equids ($n = 3$) teeth. The mean $\delta^{13}\text{C}_{\text{carb}}$ values for bovines are between -9‰ to -9.3‰ ($\delta^{13}\text{C}_{\text{diet}}$
 522 = -23.6‰ and -23.8‰), and for horses between -10‰ and -10.7‰ ($\delta^{13}\text{C}_{\text{diet}}$ = -23.7‰ and -24.4‰) (Fig.3).
 523 In this site, the $\delta^{13}\text{C}_{\text{carb}}$ values for horses are notably higher than in the Vasco-Cantabrian region (around
 524 +1-2‰) (Table 3). Both species have relatively high $\delta^{18}\text{O}_{\text{carb}}$ values, but they fall inside the range of
 525 variation observed in the Vasco-Cantabrian region, between -5.5‰ and -3.6‰ in bovines and between -
 526 4.8‰ and -4.4‰ in horses. Bovine and equid isotopic niches overlap (Fig. 4), but different responses are
 527 seen in mean $\delta^{18}\text{O}_{\text{mw}}$ values between the two bovines, with one high mean value but close $\delta^{13}\text{C}_{\text{diet}}$ mean
 528 values.

529 All individuals show flat $\delta^{13}\text{C}_{\text{carb}}$ intratooth profiles (<0.3‰ variation). Some individuals analysed do not
 530 show $\delta^{18}\text{O}_{\text{carb}}$ sinusoidal profiles, with intratooth profiles moderately flat and ranging from 1.1‰ to 1.6‰.
 531 We detect an inverse relation between $\delta^{13}\text{C}_{\text{carb}}$ and $\delta^{18}\text{O}_{\text{carb}}$ in some points of bovine individual isotopic
 532 profiles. MATs oscillated between 9.8°C and 11.9°C (MATAs = -5.4°C/-3.3°C), with summer temperatures
 533 from 16.3°C to 27.5°C and winter temperatures from -0.5°C to 1.8°C (Table 4). MAPs extend between
 534 211mm and 316mm (MAPAs = -431/-326mm). No substantial differences are noticed in the estimations
 535 based on bovines and equids because mean $\delta^{13}\text{C}$ diet values differed relatively little.

536

Site	Sam ple	Le vel	Species	MAT (°C)		Summer (°C)		Winter (°C)		Seaso nality (°C)	MAP (mm)		
				Estim ated	Rela tive	Estim ated	Rela tive	Estim ated	Rela tive		Estim ated	Rela tive	
Axlor	AXL 59	III	<i>Bos/Biso</i> <i>n sp.</i>	9.4	-2.8	17.6	-0.3	-3.9	-11.0	21.5	204	-843	
	AXL 60	III	<i>Bos/Biso</i> <i>n sp.</i>	10.8	-1.4	22.7	4.7	4.8	-2.3	17.9	300	-747	
	AXL 65	III	<i>Bos/Biso</i> <i>n sp.</i>	9.7	-2.5	22.7	4.8	-2.5	-9.6	25.2	204	-843	
	AXL 66	III	<i>Bos/Biso</i> <i>n sp.</i>	12.6	0.4	22.8	4.8	-3.2	-10.3	26.0	204	-843	
	AXL 70	IV	<i>Bos/Biso</i> <i>n sp.</i>	11.1	-1.1	21.9	3.9	-8.0	-15.1	29.9	227	-820	
	AXL 77	VI	<i>Bos/Biso</i> <i>n sp.</i>	9.1	-3.1	20.4	2.5	-10.9	-17.9	31.3	300	-747	
	AXL 86	VI	<i>Bos/Biso</i> <i>n sp.</i>	11.1	-1.1	25.9	8.0	3.1	-4.0	22.8	326	-721	
	El Castillo	CAS 141	A	<i>Bos/Biso</i> <i>n sp.</i>	11.7	-1.7	24.2	5.6	-0.8	-9.9	25.1	546	-486
		CAS 142	A	<i>Bison</i> <i>priscus</i>	12.6	-0.9	19.6	1.0	3.1	-5.9	16.5	536	-496
CAS 143		A	<i>Equus sp.</i>	5.7	-7.8	20.7	2.1	-5.6	-14.7	26.3	645	-387	
CAS 60		E	<i>Equus sp.</i>					1.6	-7.5		510	-522	
CAS 61		E	<i>Equus sp.</i>	9.7	-3.8	25.9	7.3	-4.1	-13.2	30.1	561	-471	
CAS 139		E	<i>Bos/Biso</i> <i>n sp.</i>	11.2	-2.3	18.8	0.2	1.8	-7.3	17.0	622	-410	
CAS 140		E	<i>Bos/Biso</i> <i>n sp.</i>	11.3	-2.1						602	-430	
CAS 135		C	<i>Bos/Biso</i> <i>n sp.</i>			17.0	-1.6				551	-481	
CAS 136		C	<i>Bos/Biso</i> <i>n sp.</i>	10.6	-2.9						699	-333	
CAS 137		C	<i>Bos/Biso</i> <i>n sp.</i>					0.0	-9.1		376	-656	
CAS 138		C	<i>Bos/Biso</i> <i>n sp.</i>	11.8	-1.7	18.3	-0.3	3.1	-6.0	15.3	612	-420	
CAS 132		B	<i>Bos/Biso</i> <i>n sp.</i>	9.8	-3.6	26.3	7.6	-1.2	-10.3	27.5	548	-484	
CAS 133		B	<i>Bos/Biso</i> <i>n sp.</i>					-0.1	-9.2		477	-555	
CAS 134		B	<i>Bos/Biso</i> <i>n sp.</i>					0.8	-8.3		784	-248	

	CAS	18										
	58	B	<i>Equus</i> sp.	4.6	-8.8	13.5	-5.1	-11.2	-20.3	24.7	460	-572
	CAS	18										
	59	B	<i>Equus</i> sp.	13.0	-0.5						440	-592
Labeko	LAB	IX										
Koba	38	inf	<i>Equus</i> sp.	5.2	-7.4	14.5	-4.1	-1.8	-9.1	16.2	521	-526
	LAB											
	36	IV	<i>Equus</i> sp.	7.0	-5.6	16.3	-2.3	-2.4	-9.7	18.7	448	-599
	LAB											
	42	V	<i>Equus</i> sp.	7.6	-5.0				-7.3		501	-546
			<i>Bos</i>									
	LAB		<i>primigeni</i>									
	69	V	<i>us</i>	6.3	-6.3	17.3	-1.2	-4.9	-12.2	22.2	248	-799
	LAB											
	20	VI	<i>Equus</i> sp.	9.1	-3.5	15.7	-2.9	-0.9	-8.2	16.6	517	-530
			<i>Bos</i>									
	LAB		<i>primigeni</i>									
	53	VII	<i>us</i>	11.3	-1.3	27.3	8.7	-2.4	-9.7	29.7	278	-769
			<i>Bos</i>									
	LAB		<i>primigeni</i>									
	55	VII	<i>us</i>	11.4	-1.2	26.3	7.8	1.9	-5.4	24.4	397	-650
	LAB		<i>Bos/Bison</i>									
	62	VII	<i>n</i> sp.	7.2	-5.4	20.6	2.1	-2.9	-10.2	23.5	295	-752
Canyars	CA											
	N01	I	<i>Equus</i> sp.	9.8	-5.4	16.3	-5.9	1.7	-7.5	14.6	232	-410
	CA		<i>Equus</i>									
	N02	I	<i>ferus</i>	11.9	-3.3						284	-358
	CA		<i>Equus</i>									
	N03	I	<i>ferus</i>	10.4	-4.7	18.6	-3.6	-0.5	-9.7	19.1	316	-326
			<i>Bos</i>									
	CA		<i>primigeni</i>									
	N04	I	<i>us</i>			27.5	5.3				247	-395
			<i>Bos</i>									
	CA		<i>primigeni</i>									
	N05	I	<i>us</i>	11.3	-3.9	17.5	-4.7	1.8	-7.4	15.7	211	-431
Aitzbitarte III int	AITI											
	10	V	<i>Bos/Bison</i>	13.0	-0.4	19.7	0.7	-2.9	-11.4	22.6	235	1127
Otero	OTE											
	11	IV	<i>Equus</i> sp.	8.8	-4.9	19.7	0.9	-10.4	-19.8	30.1	456	-699
	OTE											
	12	IV	<i>Equus</i> sp.	12.6	-1.0	23.8	5.0	-3.1	-12.5	26.8	400	-755

537

538 **Table 4.** Summary of paleoclimatic estimations, based on $\delta^{18}\text{O}$ for temperatures (Mean Annual
539 Temperatures, MAT; summer; winter) and in $\delta^{13}\text{C}$ for precipitation (Mean Annual Precipitations, MAP).
540 Summer and winter temperature estimations were obtained from teeth with clear seasonal profiles after
541 modelling, while MAT was averaged between summer and winter before modelling. In profiles with an
542 unclear seasonal shape, MAT was deduced from the original average of all teeth points (values marked in
543 italics). Mean error associated to temperature estimations is 5.1 ± 0.6 (see details in Appendix B).
544 Seasonality is calculated as the temperature difference between summer and winter.

545 5. Discussion

546 5.1 Diet and ecological niches: carbon ratios

547 Carbon isotopic ratios are valuable indicators for discerning past animal diets, partially influenced by the
548 physiology of the animal. Considering species trends in the studied sites, bovines have generally higher
549 mean $\delta^{13}\text{C}_{\text{carb}}$ values (from -12.4‰ to -8.9‰) than horses (from -12.6‰ to -11.3‰), whereas the red deer

550 fall within the horses' range (from -13‰ to 11.3‰). In the northeastern site of Canyars, bovines also show
551 higher mean $\delta^{13}\text{C}_{\text{carb}}$ values (-9‰ to -9.3‰) compared to horses (-10.7‰ to -10‰). These differentiated
552 isotopic ranges for equids and bovines can be potentially linked to feeding behaviour. Still, these species
553 are expected to present different basal $\delta^{13}\text{C}_{\text{carb}}$ driven by their feeding behaviour and distinct physiological
554 characteristics. Bovines, being ruminants, have been suggested in previous studies to exhibit higher $\delta^{13}\text{C}_{\text{carb}}$
555 values due to increased methane production (Cerling and Harris, 1999; Tejada-Lara et al., 2018). Therefore,
556 transforming $\delta^{13}\text{C}_{\text{carb}}$ to $\delta^{13}\text{C}_{\text{diet}}$ values using species-specific equations is crucial to mitigate the species-
557 specific impact, particularly when comparing ruminants and non-ruminants. Bovines report $\delta^{13}\text{C}_{\text{diet}}$ values
558 between -27.5‰ and -23.5‰ and horses between -26‰ and -25‰. These carbon compositions are typical
559 of animals feeding on C3 plants (commonly accepted range between -34‰ and -23‰), as can be expected
560 from high-latitude ecosystems during the Pleistocene (Bocherens, 2003; Cerling and Harris, 1999; Drucker,
561 2022).

562 Environmental factors such as light exposure, water stress, temperature fluctuations, salinity, and
563 atmospheric CO_2 changes can influence variations in $\delta^{13}\text{C}$ values in a diet primarily based on C3 plants
564 (Bocherens, 2003; Kohn, 2010). Typically, $\delta^{13}\text{C}_{\text{diet}}$ values below -27‰ ($\delta^{13}\text{C}_{\text{carb}} = -13‰$) are associated
565 with animals feeding on C3 vegetation found in closed forested environments, whereas $\delta^{13}\text{C}_{\text{diet}}$ values
566 between -27‰ and -23‰ are linked to C3 open landscapes, which could include grasslands and steppe
567 areas (Bocherens, 2003). The relatively high $\delta^{13}\text{C}_{\text{diet}}$ observed here points to animals predominantly feeding
568 in open environments. The canopy effect, characterised by a depletion in ^{13}C isotopes due to dense tree
569 cover, seems unlikely among the analysed samples since none of the individuals reported $\delta^{13}\text{C}_{\text{diet}}$ below the
570 standard cut-off of -27‰ (Drucker et al., 2008; Kohn, 2010; van der Merwe, 1991). Therefore, in general
571 terms, open mosaic landscapes, ranging from light forests to meadows and grasslands, can be inferred for
572 northwestern Iberia. Given the generally higher $\delta^{13}\text{C}_{\text{diet}}$ values reported by bovines, it is likely that they
573 were foraging in more open environments than horses and can be considered predominantly grazers.
574 Particularly, bovines from El Castillo exhibit distinct feeding behaviour compared to other Vasco-
575 Cantabrian sites, as evidenced by their lower $\delta^{13}\text{C}_{\text{diet}}$ values, indicating a potential preference for browsing
576 and feeding in closer environments, possibly in lightly forested areas. Both extinct aurochs (*Bos*
577 *primigenius*) and steppe bison (*Bison priscus*) are usually classified as grass-dominant mix-feeders during
578 the Pleistocene, although it should be noted that modern European bison (*Bison bonasus*) could include
579 browsing in their diet (Rivals et al., 2022). For aurochs, a browse-dominated mixed feeding behaviour is
580 also frequently described.

581 The $\delta^{13}\text{C}_{\text{diet}}$ range in equids also indicates feeding in open environments, suggesting a general mixed-
582 feeding pattern for the Vasco-Cantabrian region. However, individuals from northeastern Iberia are likely
583 grazing in more open environments, as evidenced by their notably higher $\delta^{13}\text{C}_{\text{diet}}$ values compared to the
584 Vasco-Cantabrian region (+1-2‰). Evaluating if other factors contribute to lower $\delta^{13}\text{C}_{\text{diet}}$ values in horses
585 is critical. In the case of equid from the Vasco-Cantabrian region, it should be considered that they have
586 been pretreated with a combination of NaClO and acetic acid, which could potentially affect the isotopic
587 values. Samples after organic removal pretreatment can potentially show either higher or lower $\delta^{13}\text{C}$ values
588 and higher $\delta^{18}\text{O}$ values based on previous experiments (Pellegrini and Snoeck, 2016; Snoeck and Pellegrini,
589 2015), with $\delta^{13}\text{C}$ values generally varying below 0.3‰. Based on the observation that horses in the Vasco-
590 Cantabrian region present lower $\delta^{13}\text{C}_{\text{carb}}$ values compared to bovines but similar mean $\delta^{18}\text{O}_{\text{carb}}$ value ranges,
591 the influence of the pre-treatment on our samples is deemed to be limited.

592 Furthermore, the high variability in $\delta^{18}\text{O}_{\text{carb}}$ values at El Castillo and Labeko Koba does not correlate with
593 a significant variation in $\delta^{13}\text{C}_{\text{carb}}$ values. Based on dental wear and stable isotopes analysis, Middle and Late
594 Pleistocene horses (*Equus ferus*) were primarily grazers, although some rare cases have been reported as
595 mixed feeders or browsers, such as at Igue des Rameaux and Schöningen (Kuitens et al., 2015; Rivals et
596 al., 2009, 2015; Uzunidis, 2020). Horse populations from northern and eastern Europe were found to be
597 browsers or mixed feeders, while those from the Mediterranean region tend to be grazers (Rivals et al.,
598 2022).

599 Finally, the few cervids included in this study exhibit $\delta^{13}\text{C}_{\text{diet}}$ values that frequently overlap with horses,
600 indicating a mixed feeding behaviour that varies from more closed environments in El Castillo to more
601 open habitats in El Otero. During the Pleistocene, the red deer (*Cervus elaphus*) exhibit a flexible, mixed-
602 feeding behaviour, consuming leaves, shrubs, forbs, grass, and sedges, similar to their present-day
603 counterparts (Merceron et al., 2021; Rivals et al., 2022). Today, this species inhabits diverse habitats
604 ranging from steppes to closed temperate forests.

605 5.2 Seasonality, mobility and water acquisition: oxygen ratios and intratooth profiles

606 Average values of $\delta^{18}\text{O}_{\text{carb}}$ in Vasco-Cantabrian individuals extend between -7.2‰ and -3.3‰ (Table 3).
607 Even if no clear species patterns in $\delta^{18}\text{O}_{\text{carb}}$ are observed, in general, bovines present slightly lower $\delta^{18}\text{O}_{\text{carb}}$
608 values from -7.2‰ to 4.8‰ than other species; horses have a significant variation from -6.6‰ to -3.3‰
609 and red deer from -6.8‰ to -4.4‰. In Canyars, both species have relatively high $\delta^{18}\text{O}_{\text{carb}}$ values that fall
610 inside the variation range observed in the Vasco-Cantabrian region, between -5.5‰ and -3.6‰ in bovines
611 and between -4.8‰ and -4.4‰ in horses. Each species shows different $\delta^{18}\text{O}_{\text{carb}}$ intratooth ranges, with
612 bovines between 1‰ and 3‰, horses mostly around 1.5‰, and red deer from 1‰ to 6‰ presenting the
613 higher ranges (Table 3; Appendix D). After applying inverse modelling to correct the dampening effect
614 (Passey et al., 2005b), the majority of teeth increase the $\delta^{18}\text{O}_{\text{carb}}$ intratooth range, between 3‰ and 8‰ for
615 bovines and 2‰ and 7‰ for horses (Appendix E). Most bovines from Axlor and Labeko Koba and horses
616 from El Castillo and El Otero exhibit well-defined sinusoidal profiles in their $\delta^{18}\text{O}_{\text{carb}}$ and large intratooth
617 individual ranges, related to the predominant consumption of water sources that reflect seasonal fluctuations
618 between summer and winter. Although not all samples consistently follow this pattern, specific intratooth
619 profiles, particularly those from bovines in El Castillo and Canyars, exhibit sharp profiles with narrow
620 ranges (<1.5‰). This phenomenon was previously reported in the region in preliminary studies conducted
621 at the sites of El Castillo (Jones et al., 2019) and in the Magdalenian levels of El Mirón cave (Geiling,
622 2020).

623 Non-sinusoidal profiles observed in the data can be attributed to various factors, including sample
624 techniques and preservation issues and the inherent variability in the original isotopic signal. Factors related
625 to sampling and methods can be connected to 1) the sampling process (e.g. too deep or too distant sampling
626 grooves); 2) the imprecision of the mass spectrometer measurements; 3) uncontrolled effects of samples
627 pretreatments; 4) diagenetic alterations affecting the carbonate fraction. However, it must be noted that
628 technical reasons, whether related to sampling or pretreatment, do not appear to impact the obtained results
629 significantly. First, this study reproduces the same intratooth sampling methods that previously yielded
630 reliable results in similar research (e.g., Pederzani et al., 2023, 2021a). Second, non-significant alterations
631 in intratooth profiles of pretreated horse samples (El Castillo, Labeko Koba, Otero) are noticed in
632 comparison to untreated bovid samples (Appendix D). Some bovid samples show these non-sinusoidal
633 profiles equally. In sites where both species are analysed, no correlation is observed between $\delta^{18}\text{O}_{\text{carb}}$ and
634 $\delta^{13}\text{C}_{\text{carb}}$. In tooth enamel, diagenetic alterations are generally less pronounced than in bone due to its higher
635 mineral content. However, carbonates within tooth enamel can be more susceptible to diagenesis and
636 recrystallisation compared to the phosphate fraction, which contains a more extensive reservoir of oxygen
637 and stronger oxygen bonds (Zazzo et al., 2004; Chenery et al., 2012; Bryant et al., 1996). The carbonate
638 content in our samples, ranging from 3.9% to 8.9%, is similar to the proportion found in modern tooth
639 enamel, suggesting no immediate indication of diagenetic alteration. Diagenesis can also be evaluated by
640 comparing the isotopic values of the carbonate and phosphate fractions in a sample, as there is a predictable
641 difference between them. However, phosphate fraction measurements were still unavailable in our study,
642 except at Axlor (Pederzani et al., 2023) where good preservation was attested. Additionally, in the case of
643 diagenetic alteration, we would expect specimens from the same archaeological levels to be affected
644 similarly, which is not the case.

645 Based on these arguments, it is suggested that the non-sinusoidal $\delta^{18}\text{O}_{\text{carb}}$ signal observed in some
646 individuals may not be attributed to poor preservation; instead, it likely reflects the original isotopic
647 signature from water input, which appears to be non-seasonal. Several factors can explain why some teeth

648 do not reflect an evident seasonal fluctuation, which could be related to animals' mobility, the isotopic
649 composition of the water sources, and seasonal buffering within those water sources (Pederzani and Britton,
650 2019). The main factors considered in our study are 1) the high mobility of the animals analysed among
651 ecosystems with different isotopic baselines due to large migrations; 2) the inland-coastal or short
652 altitudinal movements through the region, which lead to the acquisition of water from sources with different
653 isotopic signal; and 3) the acquisition of water from sources with no clear seasonal signal, such as large
654 bodies of water, rivers, groundwaters, or meltwaters. At mid-latitudes, the temperature effect is currently
655 the dominant factor. However, it is crucial to note that past changes in rainfall density (as the “amount
656 effect”; Dansgaard, 1964) cannot be dismissed from having a more significant role then, particularly during
657 glacial and arid periods. These effects, with their potential to mask temperature oscillations, underscore the
658 urgency and importance of our research in understanding and predicting climate patterns. Furthermore,
659 variability between species and within the same species, even within populations living in the same habitat,
660 is also possible. This can be attributed to multiple factors, from minor differences in foraging and drinking
661 behaviour to slight metabolic and physiological variations, including body size, metabolic rate, breathing
662 rate, moisture content of food, and faeces, among others (Hoppe et al., 2004; Kohn, 1996; Magozzi et al.,
663 2019).

664 Analyses of nitrogen and sulphur stable isotopes on ungulate bone collagen from Axlør, El Castillo and
665 Labeko Koba (Jones et al., 2018, 2019; Pederzani et al., 2023) have already revealed large variation ranges
666 linked to the existence of several microenvironments just in a few kilometres within the Vasco-Cantabria
667 region. Long migrations and long hunting distances cannot solely explain these diverse values because of
668 the range of species involved and their likely small-scale movements. In our study, the minimal $\delta^{13}\text{C}_{\text{carb}}$
669 intratooth variation within individuals (<1‰) indicates limited seasonal changes in their feeding behaviour
670 that influenced the carbon isotopic composition (Appendix D). Therefore, considering the diverse
671 topography of the Vasco-Cantabrian, characterized by steep valleys connecting the Cantabrian Cordillera
672 with the Atlantic Ocean through rivers over short distances (30-50 km), the availability in the past of a wide
673 range of water sources in small areas seems highly likely. Certain drinking behaviours can influence $\delta^{18}\text{O}$,
674 as animals may acquire water from various sources, with small streams better reflecting seasonal isotopic
675 oscillations than large lakes or evaporating ponds (see synthesis in Pederzani and Britton, 2019). Systematic
676 consumption of highly buffered water sources can significantly attenuate the final recorded signal.
677 Furthermore, rivers in the region frequently contain meltwater from snow during the winter-spring months
678 and water springs.

679 **5.3 Regional trends and ecological niches**

680 This study provides valuable insights despite the limited sample size at each archaeological level. It
681 establishes a baseline of isotopic values for northern Iberia, allowing for the evaluation of regional trends.
682 In the northwest, in the Vasco-Cantabrian region, the $\delta^{13}\text{C}_{\text{carb}}$ values obtained oscillated between -13‰ and
683 -8.9‰ and between -7.2‰ and -3.3‰ in the case of $\delta^{18}\text{O}_{\text{carb}}$ values. These values are within the range
684 expected, considering previous regional studies in ungulates (Carvalho et al., 2022; Jones et al., 2019;
685 Lécuyer et al., 2021; Pederzani et al., 2023). Although oxygen variability trends are less precise, the main
686 factor distinguishing the observed changes over time is the variation of carbon isotopic composition among
687 species and regions. The combination of mean $\delta^{13}\text{C}_{\text{diet}}$ and $\delta^{18}\text{O}_{\text{mw}}$ values (Fig. 4; 5) accentuates disparities
688 in ecological niche overlap between horses and bovines, whereas cervids and horses frequently exhibit
689 shared ecological niches. The dissimilarities between bovines and horses could be attributed to shifts in
690 feeding behaviour, which may be accompanied by ecological and environmental changes, either
691 independently or in parallel.

692 Comparing the entire dataset and across all sites, the consistently lower $\delta^{13}\text{C}_{\text{diet}}$ values in horses compared
693 to bovids throughout time suggest both animals inhabited open landscapes, with bovines exhibiting a grazer
694 preference while horses show a mix-feeding diet. Only in the Middle-to-Upper Paleolithic transition 18B
695 and 18C levels of El Castillo, an exception is observed with lower $\delta^{13}\text{C}_{\text{diet}}$ values in bovines, linked to a
696 higher browser input due to a higher habitat in closer environments, such as open forests, similar to those

697 inhabited by the horses. This generates a niche overlapping between horses and bovines, most likely
698 reflecting stable conditions that could support both species in similar ecosystems. Contrarily, in the
699 Châtelperronian and early Aurignacian levels from Labeko Koba, a clear differentiation between horses
700 and bovines is observed, mainly in $\delta^{13}\text{C}_{\text{diet}}$ values, highlighting the occupation of different parts of the
701 landscape by both species. This spatially-driven niche separation between species could result from
702 resource competition derived from an unstable climatic period, where species needed to specialise to adapt
703 to the changing conditions. Notable changes are also observed in the $\delta^{18}\text{O}_{\text{carb}}$ values from Labeko Koba
704 compared to the older El Castillo and Axlor sites, with bovines exhibiting a higher fluctuation range and
705 the lowest values in the region. These trends are consistent with values observed on bone collagen from
706 previous studies in these sites. During the Middle-to-Upper Paleolithic transition in the region, by
707 comparing horses and red deer, a decrease in mean $\delta^{13}\text{C}$ (from -21‰ to -20‰) and $\delta^{15}\text{N}$ values (from 2.5‰
708 to 6‰) in bone collagen was observed in contrast to stable red deer mean $\delta^{13}\text{C}$ (Fernández-García et al.,
709 2023; Jones et al., 2018, 2019). This decrease was previously interpreted as niche fractionation, derived
710 from an opening landscape, that drove equids into low-quality pastures compared to cervids. Pollen
711 evidence in the region suggests a prevalence of steppe vegetation and low tree cover for the Châtelperronian
712 and Aurignacian (Iriarte-Chiapusso, 2000).

713 In the same period, Canyars in the northeastern area, higher mean $\delta^{13}\text{C}_{\text{diet}}$ are observed in both species
714 (between -23.6‰ and -24.4‰), indicating a preference for more open landscapes by bovines and equids.
715 The indication of open areas could be linked to the arid climatic conditions associated with the Heinrich
716 Stadial 4, which coincides with the formation of the studied level. This predominance of open areas
717 coincides with the presence of typical steppe herbivore species, such as *Equus hydruntinus* and *Coelodonta*
718 *antiquitatis*, the microfauna and pollen taxa, and the data offered by the use-wear analysis on ungulate
719 remains identified at the site (Daura et al., 2013; López-García et al., 2022; Rivals et al., 2017).

720 Aridity is a plausible explanation for the higher niche partitioning observed in Labeko Koba and the higher
721 $\delta^{13}\text{C}_{\text{diet}}$ values found in Canyars for both species during the Aurignacian. The $\delta^{13}\text{C}_{\text{diet}}$ results of bovines
722 from Aitzbitarte III interior during the Gravettian are consistent with the trend observed in Labeko Koba,
723 where previous studies have already suggested this time to be notably arid and cold (Arrizabalaga et al.,
724 2010). Finally, in the Magdalenian level of El Otero, higher $\delta^{13}\text{C}_{\text{diet}}$ values resemble those observed in
725 Canyars. However, this time, carbon values are related to niche partitioning between horses and red deer.
726 In contrast, higher $\delta^{18}\text{O}_{\text{mw}}$ values might indicate warmer conditions but are still associated with open
727 landscapes in the Vasco-Cantabrian area.

728 **5.4 Late Pleistocene climatic evolution in Northern Iberia**

729 Carbon and oxygen isotopes were used to estimate quantitative parameters related to past temperatures and
730 precipitation. In the case of oxygen isotopic compositions, an evaluation of environmental water
731 composition can be addressed before approaching temperature estimations. When transformed to $\delta^{18}\text{O}_{\text{mw}}$
732 using species-adapted correlations and correcting bias in sea water $\delta^{18}\text{O}_{\text{mw}}$, the summer $\delta^{18}\text{O}_{\text{mw}}$ values
733 obtained from the modelled teeth range from -8.9‰ to -2.2‰ , while the winter values range from -17.1‰
734 to -8.9‰ . These values can be tentatively compared with the current trends observed in $\delta^{18}\text{O}_{\text{mw}}$ range
735 recorded by the IAEA station (IAEA/ WMO, 2022) in Santander (from -3.5‰ in summer to -6.6‰ in
736 winter) and in Barcelona (from -2.2‰ in summer to -6.3‰ in winter) and the OIPC (Bowen, 2022)
737 estimations for studied locations (from -1‰ to -9‰) (Appendix B). As observed in the present, Canyars
738 exhibit mean annual $\delta^{18}\text{O}_{\text{mw}}$ values around -8.2‰ , which is lower than the current $\delta^{18}\text{O}_{\text{mw}}$ estimated for this
739 location (-5.4‰) but higher than Labeko Koba mean annual $\delta^{18}\text{O}_{\text{mw}}$ (-9.5‰). This raises the question of
740 whether the baseline $\delta^{18}\text{O}_{\text{mw}}$ differences between Canyars and the other sites can be attributed to
741 Mediterranean influence rather than the Atlantic, assuming equivalent air circulation patterns and moisture
742 sources experienced in the past as in the present (Araguas-Araguas and Diaz Teijeiro, 2005; García-Alix et
743 al., 2021; Moreno et al., 2021). However, it's important to note that these comparisons must be approached
744 thoughtfully, considering that moisture fluxes and precipitation trends may have varied significantly during
745 the Pleistocene and the Holocene (Dansgaard, 1964; Shackleton, 1987).

746 As indicated by the climate reconstructed here, temperatures were colder, and precipitation levels were
747 notably lower in the Late Pleistocene period in this region than they are nowadays (Table 4; Appendix B).
748 From 80 to 50 ka BP, in the Mousterian levels of Axlor, temperatures were slightly colder than today, but
749 older levels showed higher differences between summer and winter temperatures. Rainfall estimations
750 exhibit an unusual arid pattern, possibly affected by bovines predominantly feeding in open areas at that
751 time. This aligns with the impact of basal feeding behaviour on rainfall estimations, as previously advised
752 by Lécuyer et al. (2021). In this case, it is not possible to isolate the effect of diet from environmental
753 interference, but previous studies have highlighted stable climatic conditions at the site (Pederzani et al.,
754 2023). Climatic reconstruction, relying on a compilation of lake sediments from northern Iberia (Moreno
755 et al., 2012) suggests that from late MIS4 to 60 ka cal BP, cold but relatively humid conditions
756 predominated, with drier conditions emerging later. Additionally, stalagmites from the Ejulve cave in the
757 Iberian range indicate a dry climate until 65.5 ka BP, preceding HE6, followed by more humid conditions
758 afterwards (Pérez-Mejías et al., 2019).

759 During the late Middle Paleolithic and early Aurignacian occupations, the observed shift in the niche
760 configuration of species suggests potential climatic perturbations. There is a decreasing trend in
761 temperatures from the Transitional Aurignacian levels in El Castillo (18C and 18B; ca. 47-46 ka cal BP) to
762 the Châtelperronian (Xinf; 45.1 ka cal BP) and Early Aurignacian (VII-V; from 40.7 to 36.3 ka cal BP)
763 levels in Labeko Koba. Lower mean annual and winter temperatures are particularly notable at El Castillo
764 and Labeko Koba. Labeko Koba levels exhibit high seasonal amplitude, especially at level VII.
765 Additionally, there is a slight decrease in rainfall and increased fluctuations from the Transitional
766 Aurignacian levels from El Castillo (18B-18C) to the Aurignacian levels in Labeko Koba (VII-V). Previous
767 studies in the northern Iberian region underlined an environmental and ecological shift after GS13/HE5,
768 from 48 to 44 ka cal BP, based on a progressive trend to colder temperatures, aridity increase, and open
769 environmental conditions, matching with the late Neanderthal occupations, followed by a population hiatus
770 before the arrival of Anatomically Modern Humans (Fernández-García et al., 2023; Vidal-Cordasco et al.,
771 2022). This episode coincides with the maximum extent of glaciers in this region, as recorded in Lake Enol
772 and Vega Comeya and a significant decrease in plant biomass and herbivore abundance around 44 to 38
773 ka BP (Ballesteros et al., 2020; Jiménez-Sánchez et al., 2013; Ruiz-Fernández et al., 2022). Moreover,
774 previous isotopic analyses in the region pointed to some ecological alterations considering perturbations
775 observed in the $\delta^{13}\text{C}$ and $\delta^{15}\text{N}$ of bone collagen (Jones et al., 2018, 2019). This tendency of increased aridity
776 aligns with observations made in regional lake sediments from northern Iberia between 60 and 23.5 ka cal
777 BP, marked by abrupt climate changes associated with HE (Moreno et al., 2012). Supporting this, the
778 marine core MD04-2845 in the northern margin of Iberia reveals a decline in the Atlantic forest and an
779 expansion of steppe and cold grasses from 47 to 40 ka BP (Fourcade et al., 2022).

780 When comparing the environmental reconstruction of the Aurignacian period between the Vasco-
781 Cantabrian (levels V-IV from Labeko Koba) and the northeastern region (Layer I from Canyars), which are
782 synchronous to HE4 (39 ka BP), this study reveals notably lower rainfall levels for the latter. This is due to
783 the feeding behaviour observed in animals, mainly in open areas. However, these drier conditions align
784 with the specific climatic conditions expected for this period and support previous findings revealing aridity
785 and the predominance of open landscapes (Daura et al., 2013; Rivals et al., 2017). The temperature data
786 indicates that, at Canyars, colder conditions were experienced, especially during the winter season,
787 compared to the present. However, in comparison to Labeko Koba, Canyars experienced warmer
788 conditions. As explained earlier, the Mediterranean basin had consistently higher temperatures, even during
789 colder periods. This is consistent with the persistence of Mediterranean open forests in the surroundings,
790 as indicated by other studies (López-García et al., 2013; Rivals et al., 2017). Continuous natural records are
791 lacking in the northeastern Iberian margin. However, the inland stalagmite record from Ejulve Cave (Pérez-
792 Mejías et al., 2019) and the sedimentary lacustrine sequence of Cañizar de Villarquemado (González-
793 Sampériz et al., 2020) have identified the most arid intervals during HE5 and HE4. These periods were
794 characterized by steppe vegetation expansions, followed by deciduous woodland expansion. To the south,

795 the Padul sequence agrees with cold and dry conditions alternating with forest recovery (Camuera et al.,
796 2019), as documented in the Alborean Sea (Martrat et al., 2004).

797 Finally, the sites Aitzbitarte III interior (27.9 ka cal BP) and El Otero (17.3 ka cal BP) provided valuable
798 climatic insights into the Vasco-Cantabrian region during the Upper Paleolithic, specifically during the
799 Gravettian and Magdalenian, respectively. Considering previous research in the region, the climatic trend
800 reported for the Aurignacian, characterised by colder and more arid conditions, was expected to continue
801 or even intensify during the Gravettian (Fernández-García et al., 2023; Garcia-Ibaibarriaga et al., 2019b;
802 Lécuyer et al., 2021). Both sites indicate lower precipitation than today in this area, indicating significant
803 aridity, with ungulates feeding predominantly in open landscapes. However, El Otero's higher mean annual
804 temperatures recorded in the Magdalenian horses respect to other sites within the Vasco-Cantabrian, are
805 consistent with a climatic amelioration following the Last Glacial Maximum (Jones et al., 2021). MIS 2 is
806 marked by the most extreme glacial conditions, as indicated by NGRIP and marine cores in Iberian margins
807 (Martrat et al., 2004; Sánchez Goñi et al., 2002). However, other regional proxies, such as lake sediment
808 and the stalagmite sequence in Pindal Cave (Moreno et al., 2010), suggest a complex and highly variable
809 climate during MIS 2. These proxies identify the coldest and most arid period within MIS 2 as the interval
810 from 18 to 14 ka cal BP rather than the global Last Glacial Maximum (23 to 19 ka cal BP).

811 **5. Conclusions**

812 This study provides a detailed analysis of the temporal evolution of the environment and climatic conditions
813 in northern Iberia, spanning from the Middle Paleolithic to the late Upper Paleolithic, this is from the GS21
814 to the GS2, ranging from 80 ka BP to 17 ka cal BP. In the Vasco-Cantabrian region, the results reveal a
815 heterogeneous open mosaic landscape, ranging from light forest to meadows and grasslands. This landscape
816 reconstruction is primarily inferred by the feeding locations of the studied animals and, consequently,
817 related to the ecosystems where hominins captured them. Despite shifts in niche configuration observed
818 between equids and bovines, both species typically foraging in open areas, with bovines showing a higher
819 preference for grazing. Only in El Castillo, during the late Mousterian and the Transitional Aurignacian
820 levels, bovines show unusually low $\delta^{13}\text{C}_{\text{diet}}$ related to higher browsing and overlapping with horse isotopic
821 niche. This might indicate a slightly closed mosaic landscape that could sustain both species. In contrast,
822 only horses from Canyars exhibit a preference for grazing behaviour.

823 Stable climatic conditions are described for Mousterian in Axlor and El Castillo levels from 80 to 50 ka cal
824 BP. However, some elements indicate environmental perturbations initiated during the Transitional
825 Aurignacian levels of El Castillo, around 48-45 ka BP and after HE5/GS13. After GS12 (44.2-43.3 ka BP),
826 horses and bovines are potentially occupying different ecological niches during the Châtelperronian and
827 early Aurignacian levels of Labeko Koba, pointing to a species' environmental specialisation, which can be
828 a consequence of competition for food resources during an unstable ecological period. The climatic
829 estimations indicate a temperature shift during this period, with a slight decrease in temperatures and
830 evidence of fluctuations in rainfall. Previous environmental studies on the region have underlined
831 ecological stress and increasing aridity from around 42.5 ka cal BP, which may relate to a broader
832 ecosystem decline. When comparing the environmental conditions during the Aurignacian period in the
833 northeast (Canyars) and the northwest (Labeko Koba), the first had higher baseline temperatures but also
834 experienced higher aridity. Animals continued to feed on open landscapes during the Gravettian and
835 Magdalenian levels in the Vasco-Cantabrian region, represented by Aitzbitarte III interior and El Otero.
836 However, there is evidence of a temperature recovery after the LGM at the El Otero.

837 The results presented here, derived from the first extensive sampling in the Vasco-Cantabrian, establish the
838 basis of future stable isotopic studies on faunal tooth enamel in Iberia. Despite the uncertainties inherent in
839 this work, both $\delta^{18}\text{O}$ and $\delta^{13}\text{C}$ contributed to the regional climatic characterisation, including the estimation
840 of temperatures and precipitations, as well as the seasonality range between summer and winter. The
841 potential influence of pretreatment effects and uncontrolled diagenetic alterations on the enamel carbonate
842 fraction has been assessed. However, complementary diagenetic tests, using new techniques like $\delta^{18}\text{O}_{\text{phos}}$

843 and FTIR analyses are advised in further works to gain more insights into sample preservation. Ongoing
844 sulphur, hydrogen and strontium studies will provide additional information on the mobility patterns of
845 animals hunted by Late Pleistocene hominins and, therefore, will help better understand the ecological and
846 environmental context occupied by Neanderthal and modern humans and their landscape use in this
847 particular region. Finally, a more comprehensive characterisation of the baseline oxygen values would also
848 enhance the environmental interpretation of the existing data.

849 **Appendices**

850 Appendices A, C, D and E are presented after bibliography. Raw data is presented in Appendix B, available
851 at https://github.com/ERC-Subsiliencia/Ungulate_enamel-carbonate

852 **Code availability**

853 R code used to perform plots, temperature and error calculations, Bayesian models code and inverse models
854 in this manuscript can be accessed at GitHub (https://github.com/ERC-Subsiliencia/Ungulate_enamel-carbonate).
855

856 **Data availability**

857 The available datasets used for this article are provided in the supplementary materials (Appendix A-E).

858 **Author contribution**

859 A.B.M.-A. got the funding and designed the research. A.B.M.-A and M.F.-G. get the permissions for
860 sampling in the regional museums. M.F.-G., K.B, and S.P. defined the analysis strategy. M.F.-G. analysed
861 the data and wrote the manuscript with critical inputs from A.B.M.-A., K.B, and S.P. J.M.G., L.A., M.F.-
862 G., and A.C. M.F.-G., L.A., J.M.G., and A.C. achieved the teeth sampling and lab sample preparation. J.D.
863 and M.S. are responsible for the excavations in Canyars and contribute to the discussion. All the authors
864 revised and commented on the manuscript.

865 **Competing interests**

866 The contact author has declared that none of the authors has any competing interests.

867 **Acknowledgements**

868 We acknowledge the Museo de Arqueología y Prehistoria de Cantabria (MUPAC), the Consejería de
869 Educación, Cultura y Deporte del Gobierno de Cantabria, the Museo de Arqueología de Bizkaia (Arkeologi
870 Museoa) and the Centro de Colecciones Patrimoniales de la Diputación Foral de Gipuzkoa (Gordailua) –
871 Provincial Government of Guipuzkoa’s Heritage Collection Centre for the access to the archaeological
872 collections. We do appreciate the work achieved by H. Reade during the initial sampling, pretreatment and
873 analyses of samples undertaken at the University of Cantabria and Cambridge. We want to thank the two
874 anonymous referees for their valuable comments, which significantly improved the quality of the paper.

875 **Financial support**

876 Funding for Vasco-Cantabria research was obtained from the Spanish Ministry of Science and Innovation
877 (PID2021-125818NB-I00, HAR2017-84997-P and HAR2012-33956), the European Research Council
878 under the European Union’s Horizon 2020 Research and Innovation Programme (grant agreement number
879 818299; SUBSILIENCIA project) and Proyecto Puente by Consejería de Educación, Cultura y Deporte del
880 Gobierno de Cantabria. Research for Canyars was funded by the Spanish Ministry of Science and
881 Innovation (PID2020-113960GB-I00), Departament de Cultura de la Generalitat de Catalunya
882 (CLT/2022/ARQ001SOLC/128) and AGAUR (SGR2021-00337). M.F.-G. is supported by the APOSTD
883 postdoctoral fellowship (CIAPOS/2022/081/AEI/10.13039/501100011033), funded by the Generalitat
884 Valenciana and the European Social Fund. S.P. was supported by a German Academy of Sciences
885 Leopoldina postdoctoral fellowship (LPDS 2021-13) during this project. M.S. benefited from financial

886 support from a Ramon y Cajal postdoctoral grant (RYC2021-032999-I) funded by the Spanish Ministry of
887 Science and Innovation and the European Union-NextGenerationEU.

888

889 **References**

- 890 Allué, E., Martínez-Moreno, J., Roy, M., Benito-Calvo, A., and Mora, R.: Montane pine forests in NE
891 Iberia during MIS 3 and MIS 2. A study based on new anthracological evidence from Cova Gran
892 (Santa Linya, Iberian Pre-Pyrenees), *Rev. Palaeobot. Palynol.*, 258, 62–72,
893 <https://doi.org/10.1016/j.revpalbo.2018.06.012>, 2018.
- 894 Álvarez-Lao, D. J., Rivals, F., Sánchez-Hernández, C., Blasco, R., and Rosell, J.: Ungulates from
895 Teixoneres Cave (Moià, Barcelona, Spain): Presence of cold-adapted elements in NE Iberia during
896 the MIS 3, *Palaeogeogr. Palaeoclimatol. Palaeoecol.*, 466, 287–302,
897 <https://doi.org/10.1016/j.palaeo.2016.11.040>, 2017.
- 898 Ambrose, S. H. and Norr, L.: Experimental Evidence for the Relationship of the Carbon Isotope Ratios of
899 Whole Diet and Dietary Protein to Those of Bone Collagen and Carbonate, in: *Prehistoric Human*
900 *Bone*, Springer Berlin Heidelberg, Berlin, Heidelberg, 1–37, [https://doi.org/10.1007/978-3-662-](https://doi.org/10.1007/978-3-662-02894-0_1)
901 [02894-0_1](https://doi.org/10.1007/978-3-662-02894-0_1), 1993.
- 902 Araguas-Araguas, L. J. and Diaz Teijeiro, M. F.: Isotope composition of precipitation and water vapour in
903 the Iberian Peninsula. First results of the Spanish Network of Isotopes in Precipitation, in: *Isotopic*
904 *Composition of Precipitation in the Mediterranean Basin in Relation to Air Circulation Patterns*
905 *and Climate*. IAEA-TECDOC-1453, Vienna, 173–190, 2005.
- 906 Balasse, M., Ambrose, S. H., Smith, A. B., and Price, T. D.: The Seasonal Mobility Model for Prehistoric
907 Herders in the South-western Cape of South Africa Assessed by Isotopic Analysis of Sheep Tooth
908 Enamel, *J. Archaeol. Sci.*, 29, 917–932, <https://doi.org/10.1006/jasc.2001.0787>, 2002.
- 909 Ballesteros, D., Álvarez-Vena, A., Monod-Del Dago, M., Rodríguez-Rodríguez, L., Sanjurjo-Sánchez, J.,
910 Álvarez-Lao, D., Pérez-Mejías, C., Valenzuela, P., DeFelipe, I., Laplana, C., Cheng, H., and
911 Jiménez-Sánchez, M.: Paleoenvironmental evolution of Picos de Europa (Spain) during marine
912 isotopic stages 5c to 3 combining glacial reconstruction, cave sedimentology and paleontological
913 findings, *Quat. Sci. Rev.*, 248, 106581, <https://doi.org/10.1016/j.quascirev.2020.106581>, 2020.
- 914 Bendrey, R., Vella, D., Zazzo, A., Balasse, M., and Lepetz, S.: Exponentially decreasing tooth growth rate
915 in horse teeth: implications for isotopic analyses, *Archaeometry*, 57, 1104–1124,
916 <https://doi.org/10.1111/arc.12151>, 2015.
- 917 Blumenthal, S. A., Cerling, T. E., Chritz, K. L., Bromage, T. G., Kozdon, R., and Valley, J. W.: Stable
918 isotope time-series in mammalian teeth: In situ $\delta^{18}\text{O}$ from the innermost enamel layer, *Geochim.*
919 *Cosmochim. Acta*, 124, 223–236, <https://doi.org/10.1016/j.gca.2013.09.032>, 2014.
- 920 Blumenthal, S. A., Cerling, T. E., Smiley, T. M., Badgley, C. E., and Plummer, T. W.: Isotopic records of
921 climate seasonality in equid teeth, *Geochim. Cosmochim. Acta*, 260, 329–348,
922 <https://doi.org/10.1016/j.gca.2019.06.037>, 2019.
- 923 Bocherens, H.: Isotopic biogeochemistry and the paleoecology of the mammoth steppe fauna, *Deinsea*, 91,
924 57–76, 2003.
- 925 Brand, W. A., Coplen, T. B., Vogl, J., Rosner, M., and Prohaska, T.: Assessment of international reference
926 materials for isotope-ratio analysis (IUPAC Technical Report), *Pure Appl. Chem.*, 86, 425–467,
927 <https://doi.org/10.1515/pac-2013-1023>, 2014.
- 928 Britton, K., Pederzani, S., Kindler, L., Roebroeks, W., Gaudzinski-Windheuser, S., Richards, M. P., and
929 Tütken, T.: Oxygen isotope analysis of Equus teeth evidences early Eemian and early Weichselian
930 palaeotemperatures at the Middle Palaeolithic site of Neumark-Nord 2, Saxony-Anhalt, Germany,
931 *Quat. Sci. Rev.*, 226, 106029, <https://doi.org/10.1016/j.quascirev.2019.106029>, 2019.
- 932 Bryant, J. D., Luz, B., and Froelich, P. N.: Oxygen isotopic composition of fossil horse tooth phosphate as
933 a record of continental paleoclimate, *Palaeogeogr. Palaeoclimatol. Palaeoecol.*, 107, 303–316,
934 [https://doi.org/10.1016/0031-0182\(94\)90102-3](https://doi.org/10.1016/0031-0182(94)90102-3), 1994.
- 935 Bryant, J. D., Koch, P. L., Froelich, P. N., Showers, W. J., and Genna, B. J.: Oxygen isotope partitioning
936 between phosphate and carbonate in mammalian apatite, *Geochim. Cosmochim. Acta*, 60, 5145–
937 5148, [https://doi.org/10.1016/S0016-7037\(96\)00308-0](https://doi.org/10.1016/S0016-7037(96)00308-0), 1996.
- 938 Camuera, J., Jiménez-Moreno, G., Ramos-Román, M. J., García-Alix, A., Toney, J. L., Anderson, R. S.,
939 Jiménez-Espejo, F., Bright, J., Webster, C., Yanes, Y., and Carrión, J. S.: Vegetation and climate
940 changes during the last two glacial-interglacial cycles in the western Mediterranean: A new long
941 pollen record from Padul (southern Iberian Peninsula), *Quat. Sci. Rev.*, 205, 86–105,

- 942 <https://doi.org/10.1016/j.quascirev.2018.12.013>, 2019.
- 943 Carvalho, M., Jones, E. L., Ellis, M. G., Cascalheira, J., Bicho, N., Meiggs, D., Benedetti, M., Friedl, L.,
944 and Haws, J.: Neanderthal palaeoecology in the late Middle Palaeolithic of western Iberia: a stable
945 isotope analysis of ungulate teeth from Lapa do Picareiro (Portugal), *J. Quat. Sci.*, 37, 300–319,
946 <https://doi.org/10.1002/jqs.3363>, 2022.
- 947 Cascalheira, J., Alcaraz-Castaño, M., Alcolea-González, J., de Andrés-Herrero, M., Arrizabalaga, A., Aura
948 Tortosa, J. E., Garcia-Ibaibarriaga, N., and Iriarte-Chiapusso, M.-J.: Paleoenvironments and
949 human adaptations during the Last Glacial Maximum in the Iberian Peninsula: A review, *Quat.*
950 *Int.*, 581–582, 28–51, <https://doi.org/10.1016/j.quaint.2020.08.005>, 2021.
- 951 Cerling, T. E. and Harris, J. M.: Carbon isotope fractionation between diet and bioapatite in ungulate
952 mammals and implications for ecological and paleoecological studies, *Oecologia*, 120, 347–363,
953 <https://doi.org/10.1007/s004420050868>, 1999.
- 954 Chappell, J. and Shackleton, N. J.: Oxygen isotopes and sea level, *Nature*, 324, 137–140,
955 <https://doi.org/10.1038/324137a0>, 1986.
- 956 Chesson, L. A., Beasley, M. M., Bartelink, E. J., Jans, M. M. E., and Berg, G. E.: Using bone bioapatite
957 yield for quality control in stable isotope analysis applications, *J. Archaeol. Sci. Reports*, 35,
958 102749, <https://doi.org/10.1016/j.jasrep.2020.102749>, 2021.
- 959 Chillón, B. S., Alberdi, M. T., Leone, G., Bonadonna, F. P., Stenni, B., and Longinelli, A.: Oxygen isotopic
960 composition of fossil equid tooth and bone phosphate: an archive of difficult interpretation,
961 *Palaeogeogr. Palaeoclimatol. Palaeoecol.*, 107, 317–328, [https://doi.org/10.1016/0031-0182\(94\)90103-1](https://doi.org/10.1016/0031-0182(94)90103-1), 1994.
- 962
- 963 Coplen, T. B.: Guidelines and recommended terms for expression of stable-isotope-ratio and gas-ratio
964 measurement results, *Rapid Commun. Mass Spectrom.*, 25, 2538–2560,
965 <https://doi.org/10.1002/rcm.5129>, 2011.
- 966 Coplen, T. B., Kendall, C., and Hopple, J.: Comparison of stable isotope reference samples, *Nature*, 302,
967 236–238, <https://doi.org/10.1038/302236a0>, 1983.
- 968 D’Angela, D. and Longinelli, A.: Oxygen isotopes in living mammal’s bone phosphate: Further results,
969 *Chem. Geol.*, 86, 75–82, 1990.
- 970 D’Errico, F. and Sánchez Goñi, M. F.: Neandertal extinction and the millennial scale climatic variability of
971 OIS 3, *Quat. Sci. Rev.*, 22, 769–788, [https://doi.org/10.1016/S0277-3791\(03\)00009-X](https://doi.org/10.1016/S0277-3791(03)00009-X), 2003.
- 972 Dansgaard, W.: Stable isotopes in precipitation, *Tellus*, XVI, 436–468, 1964.
- 973 Daura, J., Sanz, M., García, N., Allué, E., Vaquero, M., Fierro, E., Carrión, J. S., López-García, J. M.,
974 Blain, H. a., Sánchez-Marco, a., Valls, C., Albert, R. M., Fornós, J. J., Julià, R., Fullola, J. M.,
975 and Zilhão, J.: Terrasses de la Riera dels Canyars (Gavà, Barcelona): The landscape of Heinrich
976 Stadial 4 north of the “Ebro frontier” and implications for modern human dispersal into Iberia,
977 *Quat. Sci. Rev.*, 60, 26–48, <https://doi.org/10.1016/j.quascirev.2012.10.042>, 2013.
- 978 Delgado Huertas, A., Iacumin, P., Stenni, B., Sánchez Chillón, B., and Longinelli, A.: Oxygen isotope
979 variations of phosphate in mammalian bone and tooth enamel, *Geochim. Cosmochim. Acta*, 59,
980 4299–4305, [https://doi.org/10.1016/0016-7037\(95\)00286-9](https://doi.org/10.1016/0016-7037(95)00286-9), 1995.
- 981 Drucker, D. G.: The Isotopic Ecology of the Mammoth Steppe, *Annu. Rev. Earth Planet. Sci.*, 50, 395–418,
982 <https://doi.org/10.1146/annurev-earth-100821-081832>, 2022.
- 983 Drucker, D. G., Bridault, A., Hobson, K. A., Szuma, E., and Bocherens, H.: Can carbon-13 in large
984 herbivores reflect the canopy effect in temperate and boreal ecosystems? Evidence from modern
985 and ancient ungulates, *Palaeogeogr. Palaeoclimatol. Palaeoecol.*, 266, 69–82,
986 <https://doi.org/10.1016/j.palaeo.2008.03.020>, 2008.
- 987 Eggleston, S., Schmitt, J., Bereiter, B., Schneider, R., and Fischer, H.: Evolution of the stable carbon isotope
988 composition of atmospheric CO₂ over the last glacial cycle, *Paleoceanogr. Paleoclimatology*, 31,
989 434–452, <https://doi.org/10.1002/2015PA002874>, 2016.
- 990 Fagoaga, A.: Aproximacion paleoclimática y paisajística durante el MIS3 a partir del estudio de los
991 micromamíferos del yacimiento de El Salt (Alcoi, Alicante)., Universidad de Burgos, 34 pp., 2014.
- 992 Fernández-García, M., Royer, A., López-García, J. M., Bennàsar, M., Goedert, J., Fourel, F., Julien, M.-
993 A., Bañuls-Cardona, S., Rodríguez-Hidalgo, A., Vallverdú, J., and Lécuyer, C.: Unravelling the
994 oxygen isotope signal ($\delta^{18}O$) of rodent teeth from northeastern Iberia, and implications for past
995 climate reconstructions, *Quat. Sci. Rev.*, 218, 107–121,
996 <https://doi.org/10.1016/j.quascirev.2019.04.035>, 2019.
- 997 Fernández-García, M., López-García, J. M., Royer, A., Lécuyer, C., Allué, E., Burjachs, F., Chacón, M.
998 G., Saladié, P., Vallverdú, J., and Carbonell, E.: Combined palaeoecological methods using small-
999 mammal assemblages to decipher environmental context of a long-term Neanderthal settlement in
1000 northeastern Iberia, *Quat. Sci. Rev.*, 228, 106072,

- 1001 <https://doi.org/10.1016/j.quascirev.2019.106072>, 2020.
- 1002 Fernández-García, M., Vidal-Cordasco, M., Jones, J. R., and Marín-Arroyo, A. B.: Reassessing
1003 palaeoenvironmental conditions during the Middle to Upper Palaeolithic transition in the
1004 Cantabrian region (Southwestern Europe), *Quat. Sci. Rev.*, 301, 107928,
1005 <https://doi.org/10.1016/j.quascirev.2022.107928>, 2023.
- 1006 Fick, S. E. and Hijmans, R. J.: WorldClim 2: new 1-km spatial resolution climate surfaces for global land
1007 areas, *Int. J. Climatol.*, 37, 4302–4315, <https://doi.org/10.1002/joc.5086>, 2017.
- 1008 Finlayson, C. and Carrión, J. S.: Rapid ecological turnover and its impact on Neanderthal and other human
1009 populations, *Trends Ecol. Evol.*, 22, 213–222, <https://doi.org/10.1016/j.tree.2007.02.001>, 2007.
- 1010 Fourcade, T., Sánchez Goñi, M. F., Lahaye, C., Rossignol, L., and Philippe, A.: Environmental changes in
1011 SW France during the Middle to Upper Paleolithic transition from the pollen analysis of an eastern
1012 North Atlantic deep-sea core, *Quat. Res.*, 1–18, <https://doi.org/10.1017/qua.2022.21>, 2022.
- 1013 France, C. A. M., Sugiyama, N., and Aguayo, E.: Establishing a preservation index for bone, dentin, and
1014 enamel bioapatite mineral using ATR-FTIR, *J. Archaeol. Sci. Reports*, 33, 102551,
1015 <https://doi.org/10.1016/j.jasrep.2020.102551>, 2020.
- 1016 García-Alix, A., Camuera, J., Ramos-Román, M. J., Toney, J. L., Sachse, D., Schefuß, E., Jiménez-Moreno,
1017 G., Jiménez-Espejo, F. J., López-Avilés, A., Anderson, R. S., and Yanes, Y.: Paleohydrological
1018 dynamics in the Western Mediterranean during the last glacial cycle, *Glob. Planet. Change*, 202,
1019 103527, <https://doi.org/10.1016/j.gloplacha.2021.103527>, 2021.
- 1020 García-Ibaibarriaga, N., Suárez-Bilbao, A., Iriarte-Chiapusso, M. J., Arrizabalaga, A., and Murelaga, X.:
1021 Palaeoenvironmental dynamics in the Cantabrian Region during Greenland stadial 2 approached
1022 through pollen and micromammal records: State of the art, *Quat. Int.*, 506, 14–24,
1023 <https://doi.org/10.1016/j.quaint.2018.12.004>, 2019a.
- 1024 García-Ibaibarriaga, N., Suárez-Bilbao, A., Iriarte-Chiapusso, M. J., Arrizabalaga, A., and Murelaga, X.:
1025 Palaeoenvironmental dynamics in the Cantabrian Region during Greenland stadial 2 approached
1026 through pollen and micromammal records: State of the art, *Quat. Int.*, 506, 14–24,
1027 <https://doi.org/10.1016/j.quaint.2018.12.004>, 2019b.
- 1028 Geiling, J. M.: Human Ecodynamics in the Late Upper Pleistocene of Northern Spain: An Archeozoological
1029 Study of Ungulate Remains from the Lower Magdalenian and other Periods in El Mirón Cave
1030 (Cantabria), Universidad de Cantabria, 734 pp., 2020.
- 1031 González-Sampériz, P., Gil-Romera, G., García-Prieto, E., Aranbarri, J., Moreno, A., Morellón, M.,
1032 Sevilla-Callejo, M., Leunda, M., Santos, L., Franco-Múgica, F., Andrade, A., Carrión, J. S., and
1033 Valero-Garcés, B. L.: Strong continentality and effective moisture drove unforeseen vegetation
1034 dynamics since the last interglacial at inland Mediterranean areas: The Villarquemado sequence
1035 in NE Iberia, *Quat. Sci. Rev.*, 242, <https://doi.org/10.1016/j.quascirev.2020.106425>, 2020.
- 1036 Hoppe, K. A.: Correlation between the oxygen isotope ratio of North American bison teeth and local waters:
1037 Implication for paleoclimatic reconstructions, *Earth Planet. Sci. Lett.*, 244, 408–417,
1038 <https://doi.org/10.1016/j.epsl.2006.01.062>, 2006.
- 1039 Hoppe, K. A., Stover, S. M., Pascoe, J. R., and Amundson, R.: Tooth enamel biomineralization in extant
1040 horses: implications for isotopic microsampling, *Palaeogeogr. Palaeoclimatol. Palaeoecol.*, 206,
1041 355–365, <https://doi.org/10.1016/j.palaeo.2004.01.012>, 2004.
- 1042 Iacumin, P., Bocherens, H., Mariotti, A., and Longinelli, A.: Oxygen isotope analyses of co-existing
1043 carbonate and phosphate in biogenic apatite: a way to monitor diagenetic alteration of bone
1044 phosphate?, *Earth Planet. Sci. Lett.*, 142, 1–6, [https://doi.org/10.1016/0012-821X\(96\)00093-3](https://doi.org/10.1016/0012-821X(96)00093-3),
1045 1996.
- 1046 Iriarte-Chiapusso, M. J.: El entorno vegetal del yacimiento paleolítico de Labeko Koba (Arrasate, País
1047 Vasco): análisis polínico., *Labeko Koba (País Vasco). Hienas y humanos en los albores del*
1048 *Paleolítico Super.*, Munibe, 89–106, 2000.
- 1049 Jiménez-Sánchez, M., Rodríguez-Rodríguez, L., García-Ruiz, J. M., Domínguez-Cuesta, M. J., Farias, P.,
1050 Valero-Garcés, B., Moreno, A., Rico, M., and Valcárcel, M.: A review of glacial geomorphology
1051 and chronology in northern Spain: Timing and regional variability during the last glacial cycle,
1052 *Geomorphology*, 196, 50–64, <https://doi.org/10.1016/j.geomorph.2012.06.009>, 2013.
- 1053 Jones, J. R., Richards, M. P., Straus, L. G., Reade, H., Altuna, J., Mariezkurrena, K., and Marín-Arroyo, A.
1054 B.: Changing environments during the Middle-Upper Palaeolithic transition in the eastern
1055 Cantabrian Region (Spain): direct evidence from stable isotope studies on ungulate bones, *Sci.*
1056 *Rep.*, 8, 14842, <https://doi.org/10.1038/s41598-018-32493-0>, 2018.
- 1057 Jones, J. R., Richards, M. P., Reade, H., Bernaldo de Quirós, F., and Marín-Arroyo, A. B.: Multi-Isotope
1058 investigations of ungulate bones and teeth from El Castillo and Covalejos caves (Cantabria, Spain):
1059 Implications for paleoenvironment reconstructions across the Middle-Upper Palaeolithic

- 1060 transition, *J. Archaeol. Sci. Reports*, 23, 1029–1042, <https://doi.org/10.1016/j.jasrep.2018.04.014>,
1061 2019.
- 1062 Jones, J. R., Marín-Arroyo, A. B., Corchón Rodríguez, M. S., and Richards, M. P.: After the Last Glacial
1063 Maximum in the refugium of northern Iberia: Environmental shifts, demographic pressure and
1064 changing economic strategies at Las Caldas Cave (Asturias, Spain), *Quat. Sci. Rev.*, 262, 106931,
1065 <https://doi.org/10.1016/j.quascirev.2021.106931>, 2021.
- 1066 Klein, K., Weniger, G.-C., Ludwig, P., Stepanek, C., Zhang, X., Wegener, C., and Shao, Y.: Assessing
1067 climatic impact on transition from Neanderthal to anatomically modern human population on
1068 Iberian Peninsula: a macroscopic perspective, *Sci. Bull.*, 68, 1176–1186,
1069 <https://doi.org/10.1016/j.scib.2023.04.025>, 2023.
- 1070 Kohn, M. J.: Predicting animal $\delta^{18}\text{O}$: Accounting for diet and physiological adaptation, *Geochim.*
1071 *Cosmochim. Acta*, 60, 4811–4829, [https://doi.org/10.1016/S0016-7037\(96\)00240-2](https://doi.org/10.1016/S0016-7037(96)00240-2), 1996.
- 1072 Kohn, M. J.: Comment: Tooth Enamel Mineralization in Ungulates: Implications for Recovering a Primary
1073 Isotopic Time-Series, by B. H. Passey and T. E. Cerling (2002), *Geochim. Cosmochim. Acta*, 68,
1074 403–405, [https://doi.org/10.1016/S0016-7037\(03\)00443-5](https://doi.org/10.1016/S0016-7037(03)00443-5), 2004.
- 1075 Kohn, M. J.: Carbon isotope compositions of terrestrial C3 plants as indicators of (paleo)ecology and
1076 (paleo)climate, *Proc. Natl. Acad. Sci.*, 107, 19691–19695,
1077 <https://doi.org/10.1073/pnas.1004933107>, 2010.
- 1078 Lécuyer, C., Hillaire-Marcel, C., Burke, A., Julien, M.-A., and Hélie, J.-F.: Temperature and precipitation
1079 regime in LGM human refugia of southwestern Europe inferred from $\delta^{13}\text{C}$ and $\delta^{18}\text{O}$ of large
1080 mammal remains, *Quat. Sci. Rev.*, 255, 106796, <https://doi.org/10.1016/j.quascirev.2021.106796>,
1081 2021.
- 1082 Leuenberger, M., Siegenthaler, U., and Langway, C.: Carbon isotope composition of atmospheric CO_2
1083 during the last ice age from an Antarctic ice core, *Nature*, 357, 488–490,
1084 <https://doi.org/10.1038/357488a0>, 1992.
- 1085 López-García, J. M., Blain, H.-A., Bennàsar, M., Sanz, M., and Daura, J.: Heinrich event 4 characterized
1086 by terrestrial proxies in southwestern Europe, *Clim. Past*, 9, 1053–1064,
1087 <https://doi.org/10.5194/cp-9-1053-2013>, 2013.
- 1088 López-García, J. M., Blain, H.-A., Bennàsar, M., and Fernández-García, M.: Environmental and climatic
1089 context of Neanderthal occupation in southwestern Europe during MIS3 inferred from the small-
1090 vertebrate assemblages, *Quat. Int.*, 326–327, 319–328,
1091 <https://doi.org/10.1016/j.quaint.2013.09.010>, 2014.
- 1092 López-García, J. M., Blain, H. A., Fagoaga, A., Bandera, C. S., Sanz, M., and Daura, J.: Environment and
1093 climate during the Neanderthal-AMH presence in the Garraf Massif mountain range (northeastern
1094 Iberia) from the late Middle Pleistocene to Late Pleistocene inferred from small-vertebrate
1095 assemblages, *Quat. Sci. Rev.*, 288, <https://doi.org/10.1016/j.quascirev.2022.107595>, 2022.
- 1096 Luz, B., Kolodny, Y., and Horowitz, M.: Fractionation of oxygen isotopes between mammalian, *Geochim.*
1097 *Cosmochim. Acta*, 48, 1689–1693, 1984.
- 1098 Magozzi, S., Vander Zanden, H. B., Wunder, M. B., and Bowen, G. J.: Mechanistic model predicts tissue-
1099 environment relationships and trophic shifts in animal hydrogen and oxygen isotope ratios,
1100 *Oecologia*, 191, 777–789, <https://doi.org/10.1007/s00442-019-04532-8>, 2019.
- 1101 Marín-Arroyo, A. B. and Sanz-Royo, A.: What Neanderthals and AMH ate: reassessment of the subsistence
1102 across the Middle–Upper Palaeolithic transition in the Vasco-Cantabrian region of SW Europe, *J.*
1103 *Quat. Sci.*, 37, 320–334, <https://doi.org/10.1002/jqs.3291>, 2022.
- 1104 Martrat, B., Grimalt, J. O., Lopez-Martinez, C., Cacho, I., Sierro, F. J., Flores, J. A., Zahn, R., Canals, M.,
1105 Curtis, J. H., and Hodell, D. A.: Abrupt Temperature Changes in the Western Mediterranean over
1106 the Past 250,000 Years, *Science* (80-.), 306, 1762–1765,
1107 <https://doi.org/10.1126/science.1101706>, 2004.
- 1108 Merceron, G., Berlioz, E., Vonhof, H., Green, D., Garel, M., and Tütken, T.: Tooth tales told by dental diet
1109 proxies: An alpine community of sympatric ruminants as a model to decipher the ecology of fossil
1110 fauna, *Palaeogeogr. Palaeoclimatol. Palaeoecol.*, 562, 110077,
1111 <https://doi.org/10.1016/j.palaeo.2020.110077>, 2021.
- 1112 van der Merwe, N. J.: Light Stable Isotopes and the Reconstruction of Prehistoric Diets, *Proc. Br. Acad.*,
1113 77, 247–264, 1991.
- 1114 Moreno, A., Stoll, H., Jiménez-Sánchez, M., Cacho, I., Valero-Garcés, B., Ito, E., and Edwards, R. L.: A
1115 speleothem record of glacial (25–11.6 kyr BP) rapid climatic changes from northern Iberian
1116 Peninsula, *Glob. Planet. Change*, 71, 218–231, <https://doi.org/10.1016/j.gloplacha.2009.10.002>,
1117 2010.
- 1118 Moreno, A., González-Sampériz, P., Morellón, M., Valero-Garcés, B. L., and Fletcher, W. J.: Northern

- 1119 Iberian abrupt climate change dynamics during the last glacial cycle: A view from lacustrine
1120 sediments, *Quat. Sci. Rev.*, 36, 139–153, <https://doi.org/10.1016/j.quascirev.2010.06.031>, 2012.
- 1121 Moreno, A., Iglesias, M., Azorin-Molina, C., Pérez-Mejías, C., Bartolomé, M., Sancho, C., Stoll, H., Cacho,
1122 I., Frigola, J., Osácar, C., Muñoz, A., Delgado-Huertas, A., Bladé, I., and Vimeux, F.:
1123 Measurement report: Spatial variability of northern Iberian rainfall stable isotope values –
1124 investigating atmospheric controls on daily and monthly timescales, *Atmos. Chem. Phys.*, 21,
1125 10159–10177, <https://doi.org/10.5194/acp-21-10159-2021>, 2021.
- 1126 Naughton, F., Sánchez-Goñi, M. F., Desprat, S., Turon, J.-L., and Duprat, J.: Present-day and past (last 25
1127 000 years) marine pollen signal off western Iberia, *Mar. Micropaleontol.*, 62, 91–114,
1128 <https://doi.org/10.1016/j.marmicro.2006.07.006>, 2007.
- 1129 Ochando, J., Amorós, G., Carrión, J. S., Fernández, S., Munuera, M., Camuera, J., Jiménez-Moreno, G.,
1130 González-Sampériz, P., Burjachs, F., Marín-Arroyo, A. B., Roksandic, M., and Finlayson, C.:
1131 Iberian Neanderthals in forests and savannahs, *J. Quat. Sci.*, 1–28,
1132 <https://doi.org/10.1002/jqs.3339>, 2021.
- 1133 Passey, B. H. and Cerling, T. E.: Tooth enamel mineralization in ungulates: implications for recovering a
1134 primary isotopic time-series, *Geochim. Cosmochim. Acta*, 66, 3225–3234,
1135 [https://doi.org/10.1016/S0016-7037\(02\)00933-X](https://doi.org/10.1016/S0016-7037(02)00933-X), 2002.
- 1136 Passey, B. H., Robinson, T. F., Ayliffe, L. K., Cerling, T. E., Sponheimer, M., Dearing, M. D., Roeder, B.
1137 L., and Ehleringer, J. R.: Carbon isotope fractionation between diet, breath CO₂, and bioapatite in
1138 different mammals, *J. Archaeol. Sci.*, 32, 1459–1470, <https://doi.org/10.1016/j.jas.2005.03.015>,
1139 2005a.
- 1140 Passey, B. H., Cerling, T. E., Schuster, G. T., Robinson, T. F., Roeder, B. L., and Krueger, S. K.: Inverse
1141 methods for estimating primary input signals from time-averaged isotope profiles, *Geochim.
1142 Cosmochim. Acta*, 69, 4101–4116, <https://doi.org/10.1016/j.gca.2004.12.002>, 2005b.
- 1143 Pederzani, S. and Britton, K.: Oxygen isotopes in bioarchaeology: Principles and applications, challenges
1144 and opportunities, *Earth-Science Rev.*, 188, 77–107,
1145 <https://doi.org/10.1016/j.earscirev.2018.11.005>, 2019.
- 1146 Pederzani, S., Aldeias, V., Dibble, H. L., Goldberg, P., Hublin, J. J., Madelaine, S., McPherron, S. P.,
1147 Sandgathe, D., Steele, T. E., Turq, A., and Britton, K.: Reconstructing Late Pleistocene
1148 paleoclimate at the scale of human behavior: an example from the Neandertal occupation of La
1149 Ferrassie (France), *Sci. Rep.*, 11, 1–10, <https://doi.org/10.1038/s41598-020-80777-1>, 2021a.
- 1150 Pederzani, S., Britton, K., Aldeias, V., Bourgon, N., Fewlass, H., Lauer, T., McPherron, S. P., Rezek, Z.,
1151 Sirakov, N., Smith, G. M., Spasov, R., Tran, N. H., Tsanova, T., and Hublin, J. J.: Subarctic climate
1152 for the earliest *Homo sapiens* in Europe, *Sci. Adv.*, 7, 1–11,
1153 <https://doi.org/10.1126/sciadv.abi4642>, 2021b.
- 1154 Pederzani, S., Britton, K., Jones, J. R., Agudo Pérez, L., Geiling, J. M., and Marín-Arroyo, A. B.: Late
1155 Pleistocene Neanderthal exploitation of stable and mosaic ecosystems in northern Iberia shown by
1156 multi-isotope evidence, *Quat. Res.*, 1–25, <https://doi.org/10.1017/qua.2023.32>, 2023.
- 1157 Pellegrini, M. and Snoeck, C.: Comparing bioapatite carbonate pre-treatments for isotopic measurements:
1158 Part 2 — Impact on carbon and oxygen isotope compositions, *Chem. Geol.*, 420, 88–96,
1159 <https://doi.org/10.1016/j.chemgeo.2015.10.038>, 2016.
- 1160 Pellegrini, M., Lee-Thorp, J. A., and Donahue, R. E.: Exploring the variation of the $\delta^{18}O_p$ and $\delta^{18}O_c$
1161 relationship in enamel increments, *Palaeogeogr. Palaeoclimatol. Palaeoecol.*, 310, 71–83,
1162 <https://doi.org/10.1016/j.palaeo.2011.02.023>, 2011.
- 1163 Pérez-Mejías, C., Moreno, A., Sancho, C., Martín-García, R., Spötl, C., Cacho, I., Cheng, H., and Edwards,
1164 R. L.: Orbital-to-millennial scale climate variability during Marine Isotope Stages 5 to 3 in
1165 northeast Iberia, *Quat. Sci. Rev.*, 224, <https://doi.org/10.1016/j.quascirev.2019.105946>, 2019.
- 1166 Posth, C., Yu, H., Ghalichi, A., Rougier, H., Crevecoeur, I., Huang, Y., Ringbauer, H., Rohrlach, A. B.,
1167 Nägele, K., Villalba-Mouco, V., Radzeviciute, R., Ferraz, T., Stoessel, A., Tukhbatova, R.,
1168 Drucker, D. G., Lari, M., Modi, A., Vai, S., Saupe, T., Scheib, C. L., Catalano, G., Pagani, L.,
1169 Talamo, S., Fewlass, H., Klaric, L., Morala, A., Rué, M., Madelaine, S., Crépin, L., Caverne, J.-
1170 B., Bocaeage, E., Ricci, S., Boschini, F., Bayle, P., Maureille, B., Le Brun-Ricalens, F., Bordes, J.-
1171 G., Oxilia, G., Bortolini, E., Bignon-Lau, O., Debout, G., Orliac, M., Zazzo, A., Sparacello, V.,
1172 Starnini, E., Sineo, L., van der Plicht, J., Pecqueur, L., Merceron, G., Garcia, G., Leувrey, J.-M.,
1173 Garcia, C. B., Gómez-Olivencia, A., Połtowicz-Bobak, M., Bobak, D., Le Luyer, M., Storm, P.,
1174 Hoffmann, C., Kabaciński, J., Filimonova, T., Shnaider, S., Berezina, N., González-Rabanal, B.,
1175 González Morales, M. R., Marín-Arroyo, A. B., López, B., Alonso-Llamazares, C., Ronchitelli,
1176 A., Polet, C., Jadin, I., Cauwe, N., Soler, J., Coromina, N., Rufí, I., Cottiaux, R., Clark, G., Straus,
1177 L. G., Julien, M.-A., Renhart, S., Talaa, D., Benazzi, S., Romandini, M., Amkreutz, L., Bocherens,

1178 H., Wißing, C., Villotte, S., de Pablo, J. F.-L., Gómez-Puche, M., Esquembre-Bebia, M. A., Bodu,
1179 P., Smits, L., Souffi, B., Jankauskas, R., Kozakaitė, J., Cupillard, C., Benthien, H., Wehrberger,
1180 K., Schmitz, R. W., Feine, S. C., et al.: Palaeogenomics of Upper Palaeolithic to Neolithic
1181 European hunter-gatherers, *Nature*, 615, 117–126, <https://doi.org/10.1038/s41586-023-05726-0>,
1182 2023.

1183 Pryor, A. J. E., Stevens, R. E., Connell, T. C. O., and Lister, J. R.: Quantification and propagation of errors
1184 when converting vertebrate biomineral oxygen isotope data to temperature for palaeoclimate
1185 reconstruction, *Palaeogeogr. Palaeoclimatol. Palaeoecol.*, 412, 99–107,
1186 <https://doi.org/10.1016/j.palaeo.2014.07.003>, 2014.

1187 Ramsey, C. B.: Bayesian Analysis of Radiocarbon Dates, *Radiocarbon*, 51, 337–360,
1188 <https://doi.org/10.1017/S0033822200033865>, 2009.

1189 Reimer, P. J., Austin, W. E. N., Bard, E., Bayliss, A., Blackwell, P. G., Bronk Ramsey, C., Butzin, M.,
1190 Cheng, H., Edwards, R. L., Friedrich, M., Grootes, P. M., Guilderson, T. P., Hajdas, I., Heaton, T.
1191 J., Hogg, A. G., Hughen, K. A., Kromer, B., Manning, S. W., Muscheler, R., Palmer, J. G.,
1192 Pearson, C., van der Plicht, J., Reimer, R. W., Richards, D. A., Scott, E. M., Southon, J. R., Turney,
1193 C. S. M., Wacker, L., Adolphi, F., Büntgen, U., Capano, M., Fahrni, S. M., Fogtmann-Schulz, A.,
1194 Friedrich, R., Köhler, P., Kudsk, S., Miyake, F., Olsen, J., Reinig, F., Sakamoto, M., Sookdeo, A.,
1195 and Talamo, S.: The IntCal20 Northern Hemisphere Radiocarbon Age Calibration Curve (0–55
1196 cal kBP), *Radiocarbon*, 62, 725–757, <https://doi.org/10.1017/RDC.2020.41>, 2020.

1197 Rey, K., Amiot, R., Lécuyer, C., Koufos, G. D., Martineau, F., Fourel, F., Kostopoulos, D. S., and
1198 Merceron, G.: Late Miocene climatic and environmental variations in northern Greece inferred
1199 from stable isotope compositions ($\delta^{18}\text{O}$, $\delta^{13}\text{C}$) of equid teeth apatite, *Palaeogeogr.*
1200 *Palaeoclimatol. Palaeoecol.*, 388, 48–57, <https://doi.org/10.1016/j.palaeo.2013.07.021>, 2013.

1201 Rivals, F., Uzunidis, A., Sanz, M., and Daura, J.: Faunal dietary response to the Heinrich Event 4 in
1202 southwestern Europe, *Palaeogeogr. Palaeoclim. Palaeoecol.*, 473, 123–130,
1203 <https://doi.org/10.1016/j.palaeo.2017.02.033>, 2017.

1204 Rivals, F., Bocherens, H., Camarós, E., and Rosell, J.: Diet and ecological interactions in the Middle and
1205 Late Pleistocene, in: *Updating Neanderthals. Understanding Behavioural Complexity in the Late*
1206 *Middle Palaeolithic*, 39–54, 2022.

1207 Roucoux, K. H., Shackleton, N. J., Abreu, L. De, Schönfeld, J., and Tzedakis, P. C.: Combined marine
1208 mroxy and pollen analyses reveal rapid Iberian vegetation response to North Atlantic millennial-
1209 scale climate oscillations, 56, 128–132, <https://doi.org/10.1006/qres.2001.2218>, 2001.

1210 Rozanski, K., Araguás-Araguás, L., and Gonfiantini, R.: Relation Between Long-Term Trends of Oxygen-
1211 18 Isotope Composition of Precipitation and Climate, *Science (80-.)*, 258, 981–985, 1992.

1212 Rufí, I., Solés, A., Soler, J., and Soler, N.: A mammoth (*Mammuthus primigenius* Blumenbach 1799,
1213 *Proboscidea*) calf tooth from the Mousterian of Arbreda Cave (Serinyà, NE Iberian Peninsula),
1214 *Estud. Geològics*, 74, e079, <https://doi.org/10.3989/egol.43130.478>, 2018.

1215 Ruiz-Fernández, J., García-Hernández, C., and Gallinar Cañedo, D.: The glaciers of the Picos de Europa,
1216 in: *Iberia, Land of Glaciers*, Elsevier, 237–263, [https://doi.org/10.1016/B978-0-12-821941-](https://doi.org/10.1016/B978-0-12-821941-6.00012-8)
1217 [6.00012-8](https://doi.org/10.1016/B978-0-12-821941-6.00012-8), 2022.

1218 Sánchez-Goñi, M. F., Eynaud, F., Turon, J.-L., and Shackleton, N. J.: High resolution palynological record
1219 off the Iberian margin: direct land-sea correlation for the Last Interglacial complex, *Earth Planet.*
1220 *Sci. Lett.*, 171, 123–137, 1999.

1221 Sánchez-Goñi, M. F., Landais, A., Cacho, I., Duprat, J., and Rossignol, L.: Contrasting intrainterstadial
1222 climatic evolution between high and middle North Atlantic latitudes: A close-up of Greenland
1223 Interstadials 8 and 12, *Geochemistry, Geophys. Geosystems*, 10, 1–16,
1224 <https://doi.org/10.1029/2008GC002369>, 2009.

1225 Sánchez Goñi, M., Cacho, I., Turon, J., Guiot, J., Sierro, F., Peypouquet, J., Grimalt, J., and Shackleton,
1226 N.: Synchronicity between marine and terrestrial responses to millennial scale climatic variability
1227 during the last glacial period in the Mediterranean region, *Clim. Dyn.*, 19, 95–105,
1228 <https://doi.org/10.1007/s00382-001-0212-x>, 2002.

1229 Sánchez Goñi, M. F.: Regional impacts of climate change and its relevance to human evolution, *Evol. Hum.*
1230 *Sci.*, 2, e55, <https://doi.org/10.1017/ehs.2020.56>, 2020.

1231 Schmitt, J., Schneider, R., Elsig, J., Leuenberger, D., Lourantou, A., Chappellaz, J., Köhler, P., Joos, F.,
1232 Stocker, T. F., Leuenberger, M., and Fischer, H.: Carbon Isotope Constraints on the Deglacial CO
1233 2 Rise from Ice Cores, *Science (80-.)*, 336, 711–714, <https://doi.org/10.1126/science.1217161>,
1234 2012.

1235 Schrag, D. P., Adkins, J. F., McIntyre, K., Alexander, J. L., Hodell, A., Charles, C. D., and Mcmanus, J. F.:
1236 The oxygen isotopic composition of seawater during the Last Glacial Maximum, *Quat. Sci. Rev.*,

1237 21, 331–342, 2002.

1238 Sepulchre, P., Ramstein, G., Kageyama, M., Vanhaeren, M., Krinner, G., Sánchez-Gómez, M. F., and
1239 d’Errico, F.: H4 abrupt event and late Neanderthal presence in Iberia, *Earth Planet. Sci. Lett.*, 258,
1240 283–292, <https://doi.org/10.1016/j.epsl.2007.03.041>, 2007.

1241 Shackleton, N. J.: Oxygen isotopes, ice volume and sea level, *Quat. Sci. Rev.*, 6, 183–190,
1242 [https://doi.org/10.1016/0277-3791\(87\)90003-5](https://doi.org/10.1016/0277-3791(87)90003-5), 1987.

1243 Skrzypek, G., Wiśniewski, A., and Grierson, P. F.: How cold was it for Neanderthals moving to Central
1244 Europe during warm phases of the last glaciation?, *Quat. Sci. Rev.*, 30, 481–487,
1245 <https://doi.org/10.1016/j.quascirev.2010.12.018>, 2011.

1246 Skrzypek, G., Sadler, R., and Wi, A.: Reassessment of recommendations for processing mammal phosphate
1247 $\delta^{18}\text{O}$ data for paleotemperature reconstruction, *Palaeogeogr. Palaeoclimatol. Palaeoecol.*, 446,
1248 162–167, <https://doi.org/10.1016/j.palaeo.2016.01.032>, 2016.

1249 Snoeck, C. and Pellegrini, M.: Comparing bioapatite carbonate pre-treatments for isotopic measurements:
1250 Part 1—Impact on structure and chemical composition, *Chem. Geol.*, 417, 394–403,
1251 <https://doi.org/10.1016/j.chemgeo.2015.10.004>, 2015.

1252 Staubwasser, M., Dräguşin, V., Onac, B. P., Assonov, S., Ersek, V., Hoffmann, D. L., and Veres, D.: Impact
1253 of climate change on the transition of Neanderthals to modern humans in Europe, *Proc. Natl. Acad.
1254 Sci.*, 115, 9116–9121, <https://doi.org/10.1073/pnas.1808647115>, 2018.

1255 Tejada-Lara, J. V., MacFadden, B. J., Bermudez, L., Rojas, G., Salas-Gismondi, R., and Flynn, J. J.: Body
1256 mass predicts isotope enrichment in herbivorous mammals, *Proc. R. Soc. B Biol. Sci.*, 285,
1257 20181020, <https://doi.org/10.1098/rspb.2018.1020>, 2018.

1258 Timmermann, A.: Quantifying the potential causes of Neanderthal extinction: Abrupt climate change versus
1259 competition and interbreeding, *Quat. Sci. Rev.*, 238, 106331,
1260 <https://doi.org/10.1016/j.quascirev.2020.106331>, 2020.

1261 Traylor, R. B. and Kohn, M. J.: Tooth enamel maturation reequilibrates oxygen isotope compositions and
1262 supports simple sampling methods, *Geochim. Cosmochim. Acta*, 198, 32–47,
1263 <https://doi.org/10.1016/j.gca.2016.10.023>, 2017.

1264 Tütken, T., Furrer, H., and Vennemann, T. W.: Stable isotope compositions of mammoth teeth from
1265 Niederweningen, Switzerland: Implications for the Late Pleistocene climate, environment, and
1266 diet, *Quat. Int.*, 164–165, 139–150, <https://doi.org/10.1016/j.quaint.2006.09.004>, 2007.

1267 Vidal-Cordasco, M., Ocio, D., Hickler, T., and Marín-Arroyo, A. B.: Ecosystem productivity affected the
1268 spatiotemporal disappearance of Neanderthals in Iberia, *Nat. Ecol. Evol.*, 6, 1644–1657,
1269 <https://doi.org/10.1038/s41559-022-01861-5>, 2022.

1270 Zazzo, A., Bendrey, R., Vella, D., Moloney, A. P., Monahan, F. J., and Schmidt, O.: A refined sampling
1271 strategy for intra-tooth stable isotope analysis of mammalian enamel, *Geochim. Cosmochim. Acta*,
1272 84, 1–13, <https://doi.org/10.1016/j.gca.2012.01.012>, 2012.

1273

1274